Article

Cell Reports

Dental niche cells directly contribute to tooth reconstitution and morphogenesis

Graphical abstract

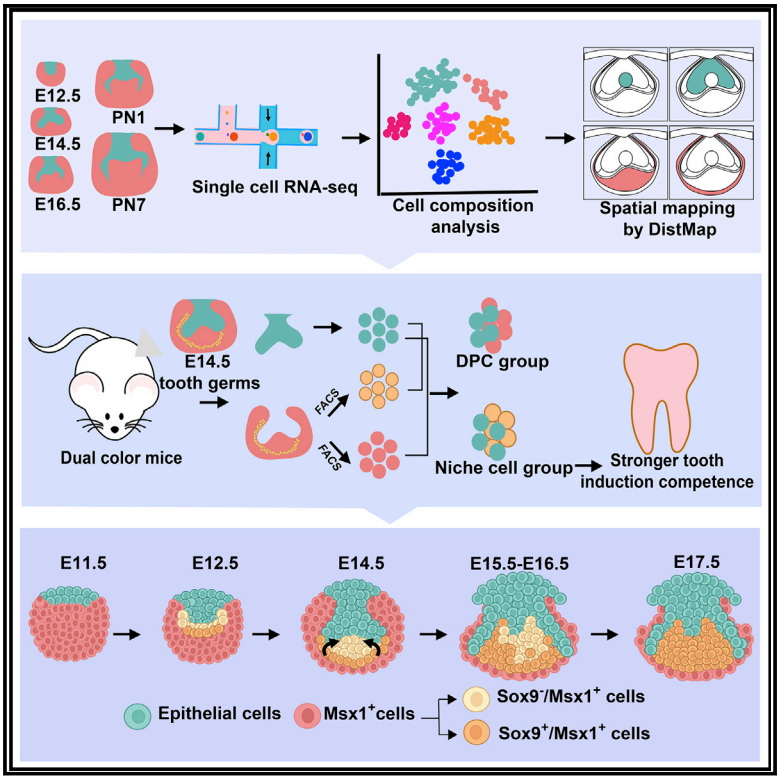

Highlights

- scRNA-seq and spatial mapping reveal cellular dynamics during mouse molar development
- Niche cells maintain robust tooth induction competence and can regenerate the papilla
- Msx1^{+}Sox9^{+} dental niche cells may be the potential cell origin for dental papilla

Authors

Hong Hu, Yufeng Duan, Kun Wang, ..., Haoyang Cai, Weidong Tian, Zhonghan Li

Correspondence

haoyang.cai@scu.edu.cn (H.C.), drtwd@sina.com (W.T.), zhonghan.li@scu.edu.cn (Z.L.)

In brief

The cellular basis for the inductive epithelial and mesenchymal interaction during tooth development remains elusive. Hu et al. dissect the cellular dynamics during mouse molar development and identify dental niche cells as the key cell composition that drives tooth induction and that Msx1^{+}Sox9^{+} niche cells may be the cell origin for the dental papilla.

Hu et al., 2022, Cell Reports *41*, 111737
December 6, 2022
https://doi.org/10.1016/j.celrep.2022.111737

CellPress

Cell Reports

CellPress
OPEN ACCESS

Article

Dental niche cells directly contribute to tooth reconstitution and morphogenesis

Hong Hu,[1,7] Yufeng Duan,[1,2,3,4,7] Kun Wang,[1,7] Huancheng Fu,[1,7] Yuansong Liao,[1] Tianshu Wang,[1] Ziwei Zhang,[1] Fanchen Kang,[1,2] Baiquan Zhang,[1] Haiying Zhang,[1] Fangjun Huo,[1,2,3] Yike Yin,[1] Guoqing Chen,[2,5] Hongbo Hu,[6] Haoyang Cai,[1,*] Weidong Tian,[1,2,3,4,*] and Zhonghan Li[1,2,8,*]

[1]State Key Laboratory of Oral Disease, West China Hospital of Stomatology, Center of Growth Metabolism and Aging, Key Laboratory of Bio-Resource and Eco-Environment of Ministry of Education, Animal Disease Prevention and Food Safety Key Laboratory of Sichuan Province, College of Life Sciences, Sichuan University, Chengdu, China

[2]National Engineering Laboratory for Oral Regenerative Medicine, West China Hospital of Stomatology, Sichuan University, Chengdu, China

[3]National Clinical Research Center for Oral Diseases, West China Hospital of Stomatology, Sichuan University, Chengdu, China

[4]Department of Oral and Maxillofacial Surgery, West China Hospital of Stomatology, Sichuan University, Chengdu, China

[5]School of Medicine, University of Electronic Science and Technology of China, Chengdu, China

[6]Department of Rheumatology and Immunology, Department of Urology, Department of Pathology, State Key Laboratory of Biotherapy, West China Hospital, Sichuan University, and Collaborative Innovation Center of Biotherapy, Chengdu, China

[7]These authors contributed equally

[8]Lead contact

*Correspondence: haoyang.cai@scu.edu.cn (H.C.), drtwd@sina.com (W.T.), zhonghan.li@scu.edu.cn (Z.L.)

https://doi.org/10.1016/j.celrep.2022.111737

SUMMARY

Mammalian teeth develop from the inductive epithelial-mesenchymal interaction, an important mechanism shared by many organs. The cellular basis for such interaction remains elusive. Here, we generate a dual-fluorescence model to track and analyze dental cells from embryonic to postnatal stages, in which Pitx2$^+$ epithelium and Msx1$^+$ mesenchyme are sufficient for tooth reconstitution. Single-cell RNA sequencing and spatial mapping further revealed critical cellular dynamics during molar development, where tooth germs are organized by Msx1$^+$Sdc1$^+$ dental papilla and surrounding dental niche. Surprisingly, niche cells are more efficient in tooth reconstitution and can directly regenerate papilla cells through interaction with dental epithelium. Finally, from the dental niche, we identify a group of previously unappreciated migratory Msx1$^+$ Sox9$^+$ cells as the potential cell origin for dental papilla. Our results indicate that the dental niche cells directly contribute to tooth organogenesis and provide critical insights into the essential cell composition for tooth engineering.

INTRODUCTION

Mammalian teeth are formed by the inductive interaction between dental epithelium and neural crest-derived ectomesenchyme. As the major organ for food crunching and pulverization, teeth are susceptible to microbe-induced erosion and cavities and aging-related enamel damage and decay, often leading to clinical root canal treatment and eventual tooth loss. Stem cell-based bioengineering strategy has offered a promising regenerative approach. It has been demonstrated that certain tissues of human teeth, such as dental pulp, could be functionally restored through stem cell-based therapies.[1] However, the dental stem cells identified so far, including SCAP (stem cells from apical papilla), SHEDs (stem cells from human exfoliated deciduous teeth), DFSCs (dental follicle stem cells), PDLSCs (periodontal ligament stem cells), DPSCs (dental pulp stem cells), and recently MDPSCs (multipotent dental pulp regenerative stem cells),[2–7] were all mesenchymal cells isolated *in vitro* at postnatal stages and did not retain the capability to initiate full tooth regeneration. On the other hand, it has long been proved that primary epithelial and mesenchymal cells from embryonic tooth germs could self-assemble and regenerate the whole tooth.[8–11] Dental mesenchyme could even induce tooth formation when combined with epithelial cells from other species,[12–14] suggesting that within the embryonic tooth germs, critical stem cell populations with tooth induction competence may exist. However, until today, the key cell composition within the developing tooth germs, especially in the mesenchyme, was still unknown, and thus, *de novo* tooth regeneration remains a challenge.

Tooth development starts from the laminal stage when the dental epithelium thickens and invades the underneath mesenchyme to form the tooth placode. The mesenchymal cells are further attracted and condensed surrounding the dental epithelium to create the initial tooth germ. The tooth germ goes through morphologically distinct stages, such as bud, cap, and bell stages, to develop into a fully functional tooth after the eruption.[15] Over the past two decades, our understanding of tooth development has been significantly increased, and multiple critical molecular regulators, often transcriptional and growth factors, have been identified using mouse genetic models. For example, BMP4 was believed to be the essential mediator of the epithelial-mesenchymal interaction due to its unique

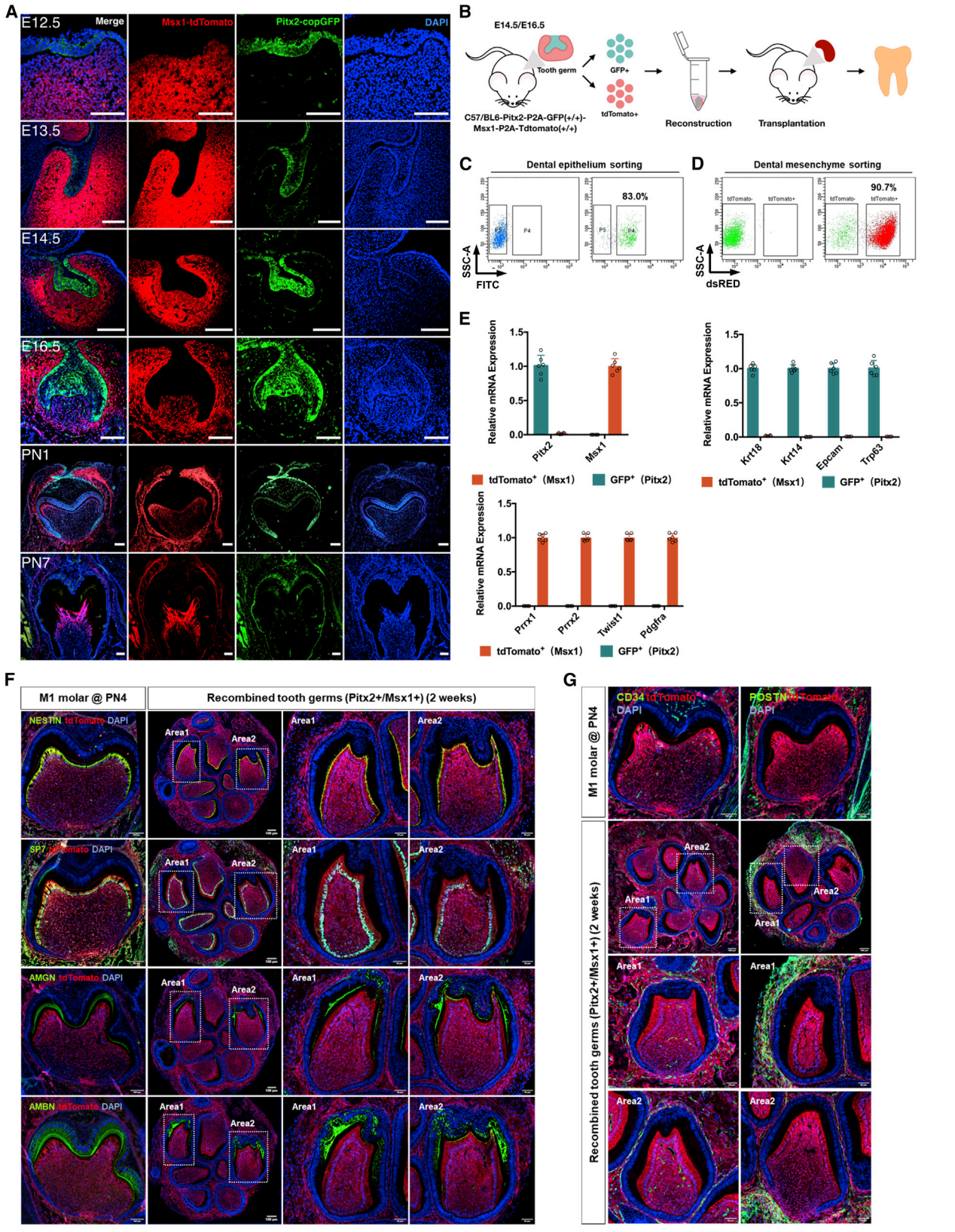

(legend on next page)

expression pattern (early expression in dental epithelium and later induced in mesenchyme).[16] Stabled Wnt/β-catenin signaling led to continuous tooth formation,[17] while Shh expression was required to promote epithelium proliferation and invasion.[18] Besides, several transcriptional factors, such as *p63*, *Lef1*, *Msx1/2*, *Lhx6/8*, *Pitx2*, *Pax9*, etc., were all involved in distinct steps of tooth development, mutation of which would cause developmental arrest at initial, bud, or cap stages.[19,20] Despite recent efforts toward dissecting the cellular mechanisms regulating tooth initiation,[21] the cellular heterogeneity of the developing tooth and the cellular basis for dental epithelial-mesenchymal interaction is still elusive. Particularly, how the tooth germ is organized and the essential cell compositions that drive the developmental process remain unknown.

The development of high-throughput single-cell transcriptomic analysis has enabled a deeper look into the cell heterogeneity of mammalian organs.[22] For example, a rare Reg4$^+$ hormone-producing intestinal cell population,[23] new Procr$^+$ progenitors in pancreas islets,[7] heterogeneous and functionally diverse human satellite cells,[24] and Wnt-secreting fibroblasts that support AT2 lung stem cells[25] were all identified through single-cell RNA sequencing (scRNA-seq) of the respective organ at various developmental stages. Besides, the emergence of novel hematopoietic and immune cell populations could be addressed by the same approach as well.[26–28] Recently, scRNA-seq has also been used in studying cell composition in the mouse incisor[29–31] as well as neural crest-derived dental lineage,[32] supporting that scRNA-seq may serve as a powerful tool to understand the composition and organization of tooth germs and could provide important insights to guide tooth engineering.

In this study, we generated a dual-fluorescence reporter knock-in mouse (Pitx2$^{P2A\text{-}copGFP}$; Msx1$^{P2A\text{-}tdTomato}$) to label and track dental cells through various developmental stages. scRNA-seq analysis revealed the cellular dynamics in dental epithelial and mesenchymal cells during molar development from embryonic day 12.5 (E12.5) to postnatal day 7 (P7). Virtual spatial mapping using DistMap[33] characterized molar-expressed genes with high accuracy, where Sdc1 was identified as a specific marker for the dental papilla, while dental niche expressed other signature genes. Surprisingly, tooth germ reconstitution experiments discovered that the niche cells exhibited much stronger tooth induction competence than the Msx1$^+$Sdc1$^+$ dental papilla by forming tooth-like structures in clusters, which was also confirmed through tooth organoid culture. Notably, the Msx1$^+$Sdc1$^+$ dental papilla cells could be directly regenerated from the interaction between epithelium and niche cells. Finally, from the dental niche, we identified a group of previously unappreciated Msx1$^+$Sox9$^+$ cells that might be the cell origin of dental papilla, which seemed to invade and replace the dental primordium during development. Together, our work revealed that dental niche cells directly contributed to tooth morphogenesis and provided important insights into the essential cell composition for efficient tooth bioengineering.

RESULTS

Generation of a dual-fluorescence model to track tooth development

Since tooth development starting from E11 to E12 is a rapid remodeling and morphogenesis process,[34] specific labeling of the developing dental epithelium and mesenchyme was a critical initial step to locate and isolate the dental progenitors for further analysis. Two developmentally important transcriptional factors, *Pitx2* and *Msx1*, were then chosen to label dental progenitor cells. The P2A-copGFP and P2A-tdTomato cassettes were knocked into the Pitx2 and Msx1 gene loci respectively (Figures S1A and S1B). Immunostaining of known Pitx2-expressing tissues such as tongue epithelium,[35] pituitary gland,[36] and eyes[37,38] confirmed that copGFP could faithfully recapitulate the *Pitx2* expression (Figure S1C). Similarly, tdTomato was also confirmed to recapitulate *Msx1* expression in the ciliary margin zone of developing retina,[39] the olfactory epithelium,[40] and the hindlimb[41] (Figure S1D). For dental cells, Pitx2-P2A-copGFP expression was able to label and track dental epithelium at various developmental stages (Figure S1E), while Msx1-P2A-tdTomato expression was specifically expressed in the dental mesenchyme (Figure S1F). These data suggested that the individual reporter knockin mice were successfully established, and the two signature transcription factors (TFs) could indeed track the development of dental epithelium and mesenchyme respectively.

To track dental epithelium and mesenchyme simultaneously, a dual-fluorescence line (Pitx2$^{P2A\text{-}copGFP}$; Msx1$^{P2A\text{-}tdTomato}$) was generated (Figure S2A). Fluorescent imaging revealed that from E10.5 to P7, both copGFP and tdTomato could efficiently label early dental tissues in the first pharyngeal arch and the developing teeth in the mandible (Figure S2B). Tissue sectioning and imaging further confirmed that molar epithelium and mesenchyme could be efficiently labeled by copGFP and tdTomato respectively (Figure 1A), as well as the incisor epithelium and mesenchyme at different developmental stages (Figure S2C).

To further characterize the labeled dental epithelium and mesenchyme, flow cytometry analysis of primary cells from

Figure 1. Efficient labeling of dental epithelium and mesenchyme by a dual-fluorescence mouse model

(A) Specific labeling of molar dental epithelium and mesenchyme across developmental stages by Pitx2-copGFP and Msx1-tdTomato, respectively. Frozen sections of tooth germs from E12.5 to P7 were analyzed by immunostaining for copGFP and tdTomato. DAPI: nuclear staining. Scale bars: 100 μm.

(B) Schematic of tooth germ reconstitution. Tooth germs at E14.5 or E16.5 were isolated for FACS sorting and tooth reconstitution from homozygous Pitx2$^{P2A\text{-}GFP}$; Msx1$^{P2A\text{-}tdTomato}$ mice. The recombinants were transplanted in the renal capsule for 2–4 weeks before analysis.

(C and D) A high percentage of Pitx2$^+$ (copGFP$^+$) epithelial cells and Msx1$^+$ (tdTomato$^+$) mesenchymal cells could be detected in E14.5 tooth germs. Wild-type cells (WT): negative control.

(E) Expressions of Pitx2, Msx1, and marker genes were confirmed by qRT-PCR. Epithelial markers: Epcam, Krt14, Krt18, and Trp63. Mesenchymal markers: Prrx1/2, Twist1, and Pdgfra. Error bars represent the standard deviation (SD) from two independent experiments with triplicates.

(F and G) Reconstituted tooth germs from Msx1$^+$ and Pitx2$^+$ cells had normal anatomy compared with the native molar tooth (P4). Samples were collected after 2 weeks of kidney capsule transplantation. M1 molar at P4 served as the positive control. Enamel: AMBN, AMGN. Odontoblasts: SP7, NESTIN. Periodontal tissues: POSTN. Endothelial cells: CD34. Scale bar: whole 100 μm, zoom-in 50 μm.

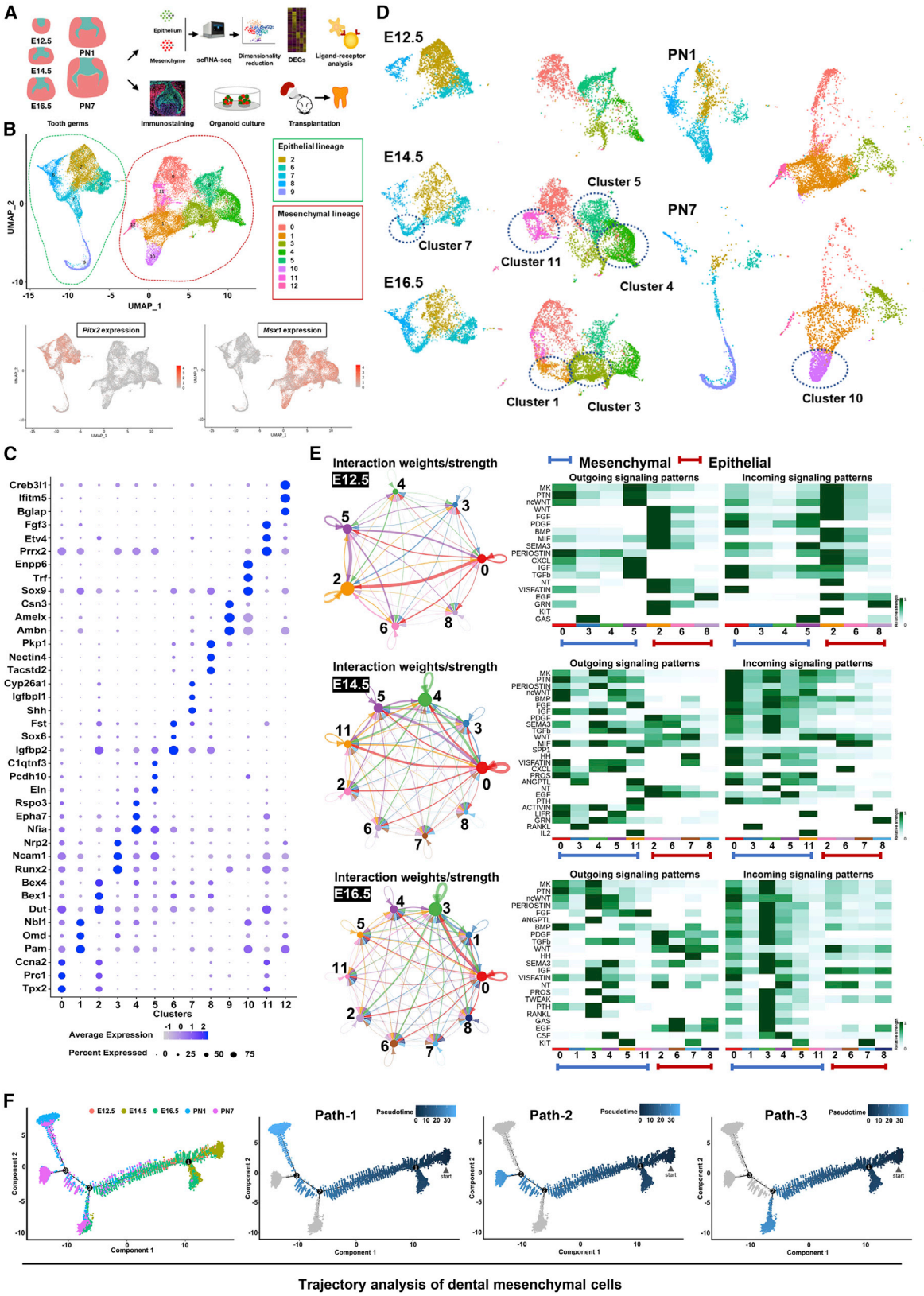

Trajectory analysis of dental mesenchymal cells

(legend on next page)

E12.5 and E16.5 indicated that although most of the dental epithelium and mesenchyme (both in molar and incisor) were copGFP$^+$ and tdTomato$^+$ respectively, a small but significant portion of cells was copGFP or tdTomato negative (Figure S2D). We reasoned that these cells might be either from the endothelial lineage, as they were reported to be present in dental niche regions as early as the cap stage,[42] or some previously uncharacterized cells within the early dental epithelium and mesenchyme.

Pitx2$^+$ epithelial and Msx1$^+$ mesenchymal cells were sufficient for tooth germ reconstitution

Although the mouse has a more simplified tooth patterning than humans, similar molecular and cellular processes are shared between mouse molar development and human dentition.[15] The incisor has long been used as a continuous tooth development model, and much less is known for molar development. Therefore, we decided to focus on dissecting the key cellular dynamics during molar development.

As mentioned above, some fluorescence-negative cells were present in the primary tooth germs. Thus, we first asked if Pitx2$^+$ epithelial and Msx1$^+$ mesenchymal cells would have full capability to reconstitute tooth germs without contribution from other cells. Primary copGFP$^+$ (Pitx2$^+$) epithelial and tdTomato$^+$ (Msx1$^+$) mesenchymal cells were isolated from mouse molars by fluorescence-activated cell sorting (FACS) and then used for tooth germ reconstitution *in vitro* and kidney capsule transplantation *in vivo* (Figure 1B). The enrichment of copGFP$^+$ and tdTomato$^+$ cells (E14.5) was validated by FACS (Figures 1C and 1D). Specific expressions of *Pitx2* and *Msx1* as well as epithelial and mesenchymal markers were all confirmed by qRT-PCR in respective isolated cell populations (Figure 1E). These data suggested that Pitx2$^+$ dental epithelial and Msx1$^+$ mesenchymal cells could be efficiently isolated.

Sorted Pitx2$^+$ (copGFP$^+$) and Msx1$^+$ (tdTomato$^+$) cells were then used for tooth reconstitution. Recombined tooth germs were transplanted under the kidney capsule for 2–4 weeks before analysis. We first tested copGFP$^+$ and tdTomato$^+$ cells at E14.5, and Micro-CT analysis indicated that the reconstituted tooth germ could develop into tooth-like structures *in vivo* (Figure S3A). Tissue sectioning and H&E staining further confirmed that the transplants contained correct dental tissues, including enamel, dental pulp, and blood vessels (Figure S3B). Immunostaining with dental markers, including Nestin and Sp7 for odontoblasts,[43–46] amelogenin (AMGN) and ameloblastin (AMBN) for enamel matrix,[47,48] periostin for periodontal cells,[49] and CD34 for dental endothelial cells,[50] all confirmed that tooth-like structures had normal anatomy comparing with the native molar tooth (M1) (Figures 1F and 1G). Furthermore, cells from E16.5 tooth germs could retain the same capability (Figure S3C), as well as primary tissues from E11.5 embryos (Figures S3D and S3E). However, things changed dramatically at postnatal stages, as the cells from P1, for example, could only generate irregular bone-like tissues, suggesting that Pitx2$^+$ and Msx1$^+$ cells had lost their tooth formation competence at this stage (Figures S3F and S3G). Together, these data indicated that embryonic Pitx2$^+$ epithelial and Msx1$^+$ mesenchymal cells contained the essential cell composition to reconstitute tooth germs, and this capability was lost at postnatal stages.

scRNA-seq revealed critical cellular dynamics of molar development

To dissect the key cell composition for tooth reconstitution, single-cell transcriptomic analysis was carried out on these cells throughout molar development, covering from E12.5, E14.5, and E16.5 to P1 and P7. The data were then subjected to bioinformatic analysis and functional validation (Figure 2A).

scRNA-seq data were first integrated using Seurat V3[22] and analyzed for pseudotime trajectory by Monocle2.[51] Thirteen main representative cell clusters were identified from the five developmental stages. Five clusters were grouped as Pitx2$^+$ epithelial cells, and eight as Msx1$^+$ mesenchymal cells, with their top differentially expressed genes listed (Figures 2B and 2C). Stage-by-stage analysis revealed that during embryonic stages, both dental epithelial and mesenchymal cells were relatively stable, as most of the cell clusters were maintained the same (clusters 0, 4, and 5, for example) (Figure 2D). At E14.5, cluster 11 (Fgf3$^+$) emerged, which probably represented dental papilla precursors.[52] While at E16.5, there was a significant increase of cluster 3 (Runx2$^+$) and the emergence of cluster 1 cells (Pam$^+$). Cluster 1 might represent pre-odontoblasts, as Pam was previously found in those cells.[53] At postnatal stages, mesenchymal cells underwent dramatic differentiation, with emergence of clusters 10 (Enpp6$^+$) and 12 (Creb3l1$^+$) with almost complete loss of clusters 4 (Epha7$^+$) and 5 (C1qtnf3$^+$) and significant decrease of cluster 0 (Ccna2$^+$) cells. Interestingly, the disappearance of cluster 4 and 5 cells was highly correlated with the loss of tooth reconstitution capability of dental mesenchyme.

CellChat[54] was then used to explore the signaling interaction of cell clusters at each stage, from which dental mesenchymal cells exhibited strong interaction both among themselves and with epithelial cells during the molar development (Figures 2E and S4A), consistent with the previous observation that tooth induction potential was transferred to dental mesenchyme after E11.[34] Among mesenchymal cell clusters, clusters 0, 4, and 5

Figure 2. Global cellular dynamics analysis of tooth germs by scRNA-seq

(A) Schematic of experimental procedures. Tooth germs were collected at from the bud stage (E12.5), cap stage (E14.5), bell stage (E16.5), postnatal day 1 (P1), and day 7 (P7) for scRNA-seq.

(B) Two-dimensional representation for epithelium and mesenchyme of integrated molars from five stages via UMAP. Epithelial and mesenchymal lineages were separated by Pitx2 and Msx1 expression.

(C) Top three featured gene expression in different cell clusters.

(D) Stage-by-stage representation of cell clusters via UMAP.

(E) CellChat analysis of intercellular communication network of secretory and received signals from E12.5 to E16.5.

(F) Pseudotime analysis by Monocle2 revealed distinct developmental paths for molar mesenchymal cells. The numbers in the figure represented the branching point of the developing cells.

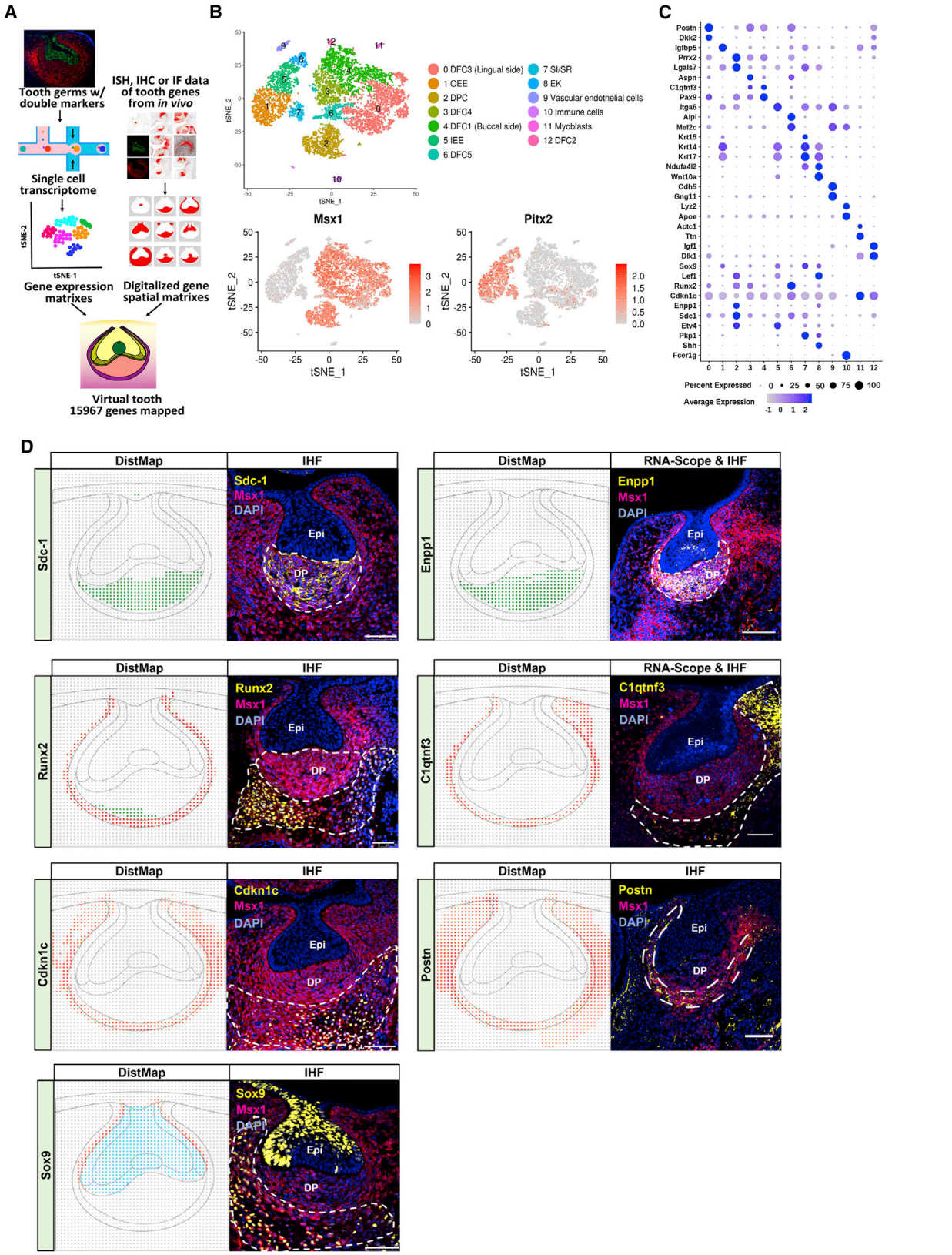

(legend on next page)

seemed to coordinate together to form outgoing signaling patterns, which not only sent autocrine signals to themselves and other mesenchymal cells but also provided critical signals to epithelial cells, such as MK, PTN, CXCL and periostin at E12.5 and CXCL, MIF, ACTIVIN and GRN at E14.5 (Figure S4B). Meanwhile, considerable outgoing and incoming signal expression dynamics were also observed among epithelial and mesenchymal cell clusters (Figure 2E).

To map the cell fate, pseudotime trajectory analysis by Monocle2 identified the different cell dynamics between the epithelial and mesenchymal lineages. Notably, epithelial cells were aligned in a linear trajectory, while mesenchymal cells exhibited multiple branches, indicating that the cells underwent several cell fate divergences during molar development (Figures 2F and S5A). For epithelial cells, those from E12.5 to 16.5 were largely aligned together and became more differentiated at postnatal stages, especially at P7, where cells were clustered at the end of the trajectory map (Figure S5A). While for mesenchymal cells, their differentiation started earlier than epithelial lineage, with E12.5–E14.5 aligned together and cells from E16.5 located in a slightly more differentiated state (Figure 2F). Again, cells from postnatal stages represented the most differentiated state in the trajectory map. Pseudotime trajectory analysis indicated three potential developmental paths (Figure 2F). For each path, GeneSwitches[55,56] was used to identify ordered critical gene expression changes over pseudotime (Figure S5B). Interestingly, activation of *Tle5* (*Aes*) was shared by all three paths. Following *Tle5* activation came the inactivation of craniofacial genes, such as *Six1/2*,[57] *Lhx8*,[58] and *Prrx1*,[59] and then the activation of other dental differentiation-associated genes at later stages. For paths 1 and 2, one of the key intermediate TFs was *Msx2*, which was ON at the E16.5 stage (Figures 2F and S5B). Msx2 knockout mice did not exhibit any developmental defects before the cap stage,[60] suggesting that paths 1 and 2 might represent the later development of dental mesenchyme. With the activation of *Runx3*, a suppressor of osteoblast differentiation,[61] path 1 might represent the developmental path for the dental pulp. For path 2, the activation of *Vdr* suggested that it represented the development of the root and crown.[62] Path 3 ended around E16.5 and showed the activation of *Cdkn1a*[63] and *Nr4a3*,[64] suggesting that it represented the development of odontoblasts. We also used additional analysis tools to further confirm these observations. CytoTRACE[65] and CellRank[66] analysis identified key progenitor groups within the integrated cell clusters and their developmental paths. Whereas epithelial cells exhibited a unidirectional differentiation path, mesenchymal cells again showed three directions (Figure S5C), like Monocle2 analysis. Together, these data suggested that during molar development, mesenchymal cells exited from the original craniofacial mesenchymal fate and initiated dental commitment-associated gene networks. At embryonic stages, the primary developmental process might be the morphogenesis of tooth germs and the accumulation of dental progenitors. The disappearance of key cell clusters at postnatal stages might trigger the differentiation of dental progenitors and the loss of tooth reconstitution capability.

Spatial mapping and pseudotime trajectory analysis suggested a central role of dental niche cells in tooth induction

As mentioned earlier, only embryonic Msx1$^+$ and Pitx2$^+$ cells were able to reconstitute complete tooth germs, but not postnatal ones (Figures S3 and S4). From scRNA-seq data, some cell clusters, such as clusters 4 (Epha7$^+$) and 5 (C1qtnf3$^+$), almost completely disappeared at postnatal stages (Figure 2D). Thus, we decided to focus on individual stages first to dissect the cell identity and developmental potential of different cell clusters.

One of the outstanding limitations of scRNA-seq was the loss of spatial information during tissue dissociation and sample preparation. To restore the spatial localization of cell clusters identified from the developing tooth germs, we started with E14.5, which is one of the most characterized dental developmental stages. *In situ* hybridization (ISH), immunohistochemistry (IHC), and immunofluorescence (IF) data of E14.5 tooth-associated signature genes were collected from the public domains to create a digitalized gene spatial matrix (Figure S6A). DistMap[33] was then utilized to generate a virtual tooth model (Figure 3A). From E14.5 scRNA-seq data, 13 cell clusters with their respective signature genes were characterized (Figures 3B and 3C). Then, we used the virtual tooth model to map the signature gene profiles of each cell cluster and visualize their spatial localization. Indeed, the model could efficiently restore the spatial information for each cell group and allocate them accordingly in the virtual molar (Figure S6B). Notably, we found that in the dental mesenchyme, besides identifying Sdc1 and Enpp1 as surface markers that specifically localized to the dental papilla region (Figure 3D, top panel), many genes exhibited distinct expression patterns in the dental niche. Several representative ones were chosen for validation by RNA-scope and immunostaining, including *Runx2*, *C1qtnf3*, *Cdkn1c*, *Postn*, and *Sox9* (Figure 3D). Among them, *Runx2* exhibited strong signals in the bottom niche region surrounding the dental papilla but also was lightly detectable in the papilla itself. *C1qtnf3*, a marker gene for cluster 5 in the integrated datasets (Figure 2C), was

Figure 3. Spatial mapping of single-cell transcriptome by DistMap

(A) Schematic procedure for constructing the virtual tooth and spatial mapping of cell clusters. Existing data for dental marker genes (103 genes) at E14.5 were quality checked before extraction from published domains for digitalization. Digitalized spatial matrixes were drawn, and the gene expression profile of the scRNA-seq dataset was then spatially mapped to the virtual tooth. In total, about 15,967 genes expressed at E14.5 could be specifically mapped in the model.

(B) Two-dimensional representation of E14.5 molar via tSNE. IEE, inner enamel epithelium; DPC, dental papilla cells; DFC1-5, dental follicle cells 1–5; OEE, outer enamel epithelium; SI/SR, intermedium stratum cells/satellite reticulum; EK, enamel knot.

(C) Representative featured marker genes expressed in each cell cluster.

(D) Immunohistofluorescence (IHF) and RNA-scope analysis confirmed the predicted localization of maker genes at E14.5. DAPI: nuclear staining. DistMap: green, papilla; red, niche; blue, epithelium. Msx1$^+$ regions: anti-tdTomato. IgG: negative control. Scale bars: 75 μm (Cdkn1c, Postn, Sdc1, Sox9), 50 μm (Runx2, C1qtnf3, Enpp1).

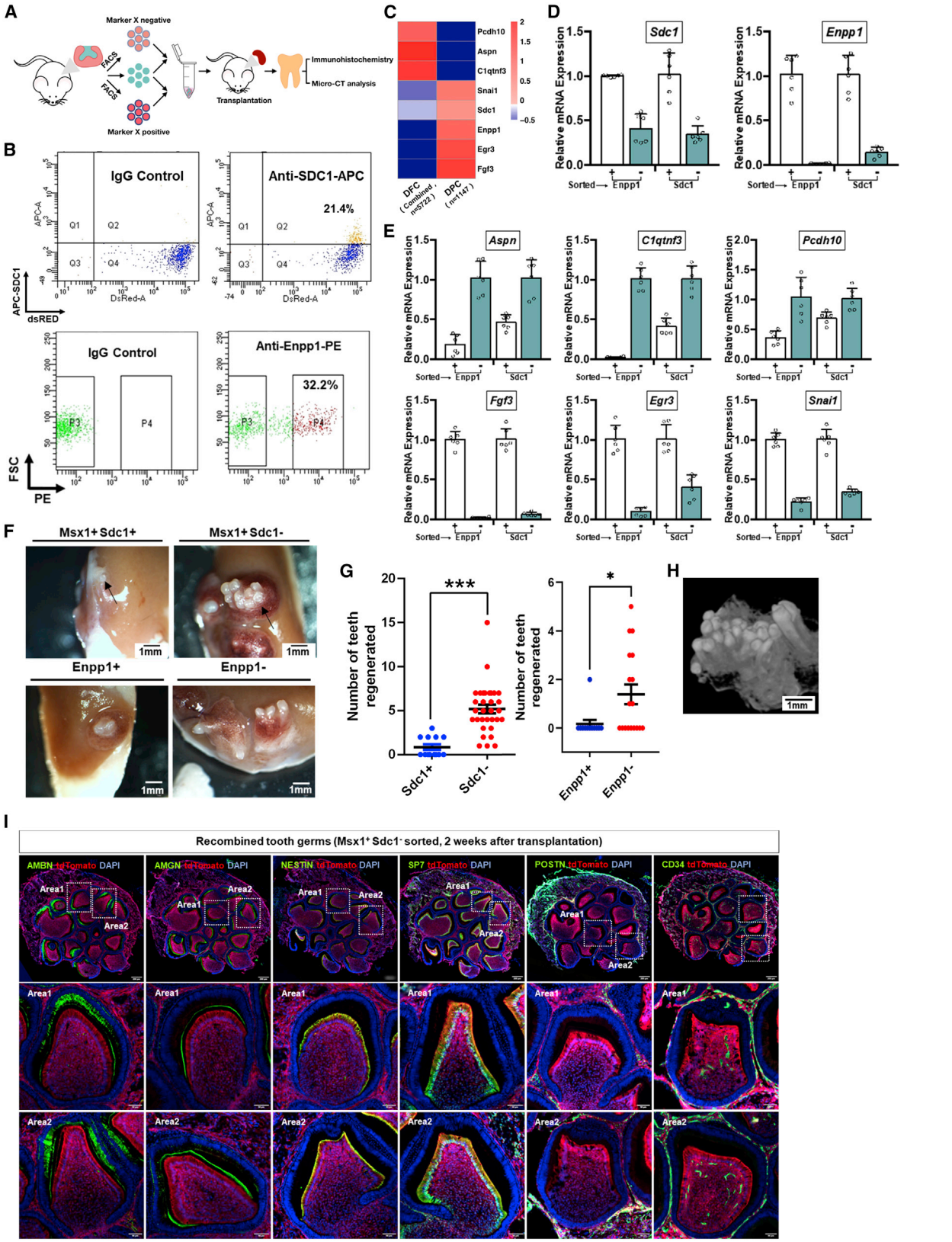

(legend on next page)

present only in the niche with strong signals in the top buccal side. *Cdkn1c* and *Postn* were all expressed in the niche but also detectable in the distal regions. *Sox9* could be detected from both epithelial and niche regions. Given the various gene patterns in dental niche cells, we then tried to analyze their cell fate relationship with the dental papilla cells. Pseudotime trajectory analysis revealed that dental niche cells (marked by *Cdkn1c*, *Postn*, and *C1qtnf3*), represented an earlier state than dental papilla (marked by *Enpp1* and *Sdc1*) (Figures S7A and S7B), which was also confirmed by another independent method, VECTOR[67] (Figure S7C). Together, these data suggested that significant cellular diversity existed in dental niche cells, and some of them might be in a progenitor state compared with dental papilla cells.

Dental niche cells were the critical cell composition for tooth germ reconstitution

To investigate which cell cluster might possess the tooth induction capability, we first separated E14.5 dental mesenchyme into two groups, dental papilla cells and dental niche, by flow cytometry and then used them for tooth reconstitution with dental epithelium (Figure 4A). As mentioned earlier, DistMap analysis and IHC both confirmed that Sdc1 and Enpp1 were specifically expressed in the dental papilla region at E14.5 (Figure 3D). Flow cytometry was then used to isolated Sdc1$^+$ and Enpp1$^+$ cells (Figure 4B). From scRNA-seq data, a list of marker genes specifically expressed in the dental papilla and niche cells was identified and used to confirm cell sorting (Figure 4C). Indeed, dental papilla (Msx1$^+$ Sdc1$^+$ or Msx1$^+$ Enpp1$^+$) and dental niche (Msx1$^+$ Sdc1$^-$ or Msx1$^+$ Enpp1$^-$) could be efficiently separated by FACS (Figure 4D), and the sorted cells were correctly enriched with dental papilla and follicle niche markers respectively (Figure 4E).

To reconstitute the tooth germ, the same number of sorted cells were mixed with primary dental epithelial cells and then transplanted in the kidney capsule for 2–4 weeks. Surprisingly, clusters of teeth were formed in the Msx1$^+$ Sdc1$^-$ and Msx1$^+$ Enpp1$^-$ dental niche groups, while the dental papilla group only exhibited minimal capability (Figure 4F). Most of the recombinants from the dental papilla group could not generate any tooth-like structures, while dental niche cells possessed much higher induction competence (Figure 4G). Moreover, the Micro-CT scan indicated that the tooth-like structures from the dental follicle group contained mineralized tissues (Figure 4H), and H&E staining showed that these structures formed various dental tissues, including dental pulp, dentin, enamel, and periodontal ligament (Figure S8A). Immunostaining with dental markers also confirmed that the tooth-like structures had normal anatomy (Figure 4I). Together, these data strongly supported that the dental niche cells were enriched with a stem cell population that interacted with dental epithelium to promote tooth formation.

Dental niche cells promoted epithelium reorganization and survival during tooth reconstitution

To investigate how dental niche cells could promote tooth formation in clusters, a tooth organoid culture system was first established *in vitro*. In normal conditions, recombined dental epithelium would undergo fast reorganization and form multiple foci (days 3–7) (Figure S8B). Frozen sectioning and confocal analysis revealed that tooth germ-like structures could be spotted as early as day 6 (Figure S8C). On day 24, the derivation of ameloblasts (Figure S8D) and formation of enamel tissue (Figure S8E) could be detected. Therefore, we concluded that the organoid culture system could be used to track and characterize tooth germ formation *in vitro*.

When sorted cells were recombined with dental epithelium to form reconstituted tooth germs, only niche cells (Msx1$^+$Sdc1$^-$) could promote the reorganization of the dental epithelium in the same way as wild-type controls, while dental papilla cells (Msx1$^+$ Sdc1$^+$) failed to do so (Figure 5A). Moreover, only organoids from the dental niche group could develop normally for at least 2 weeks (Figure 5B), and Sdc1$^+$ dental papilla cells were regenerated from the recombined tooth germs (Figure 5C). Similar results could also be obtained in sorted Msx1$^+$Enpp1$^-$ dental niche cells (Figures 5D–5F). In addition, when transplanted on day 10, only organoids from the dental niche group could generate tooth-like structures *in vivo* (Figure 5G), which contained multiple dental tissues, including enamel, dentin, dental pulp, and blood vessels (Figure 5H). Together, these data further supported that the dental niche cells contained the key stem cells that interacted with dental epithelium and induced tooth reconstitution.

Msx1$^+$ Sox9$^+$ dental niche cells might play a central role in tooth morphogenesis

To investigate the development of dental papilla *in vivo*, we first examined *Sdc1* expression in tooth germs at different stages. Sdc1 was first observed in a small group of Msx1$^+$ mesenchymal cells immediately below the invading dental epithelium at E12.5

Figure 4. Niche cells exhibited a stronger capability to reconstitute tooth germs than dental papilla ones

(A) Overall experimental procedure. Epithelial cells were sorted by copGFP. Mesenchymal cells were sorted by both tdTomato and one additional surface marker (Sdc1 or Enpp1). Sorted cells were then mixed to reconstitute tooth germs.

(B) Sorting of Sdc1$^+$/Enpp1$^+$ and Sdc1$^-$/Enpp1$^-$ cells by flow cytometry. Primary cells were immunostained with anti-Sdc1-APC or anti-Enpp1-PE antibodies before sorting. IgG: negative control.

(C) Heatmap image for marker genes specifically expressed in dental follicle niche cells (DFCs) and dental papilla cells (DPCs) from scRNA-seq.

(D and E) Confirmation of Sdc1, Enpp1, and marker gene expression in sorted cells. Error bars represent SD from two independent experiments with triplicates.

(F) Representative images of tooth formation by Msx1$^+$ Sdc1$^-$ and Msx1$^+$ Enpp1$^-$ cells. Samples were analyzed 4 weeks after transplantation.

(G) Msx1$^+$Sdc1$^-$ and Msx1$^+$Enpp1$^-$ niche cells exhibited stronger tooth inducing capability than Msx1$^+$Sdc1$^+$ and Msx1$^+$Enpp1$^+$ cells. Msx1$^+$Sdc1$^-$, n = 32; Msx1$^+$Sdc1$^+$, n = 13. Msx1$^+$ Enpp1$^+$, n = 11; Msx1$^+$Enpp1$^-$, n = 18. Statistics: independent samples t test by SPSS. *$p < 0.05$, ***$p < 0.001$. Error bar: mean ± SEM.

(H) Micro-CT analysis confirmed the mineralization of reconstituted teeth by Msx1$^+$Sdc1$^-$ cells. Samples were collected 4 weeks after transplantation.

(I) Reconstituted tooth germs from sorted Msx1$^+$Sdc1$^-$ cells had normal tooth anatomy. Samples were collected 2 weeks after transplantation. Enamel markers: AMGN, AMBN. Odontoblasts: NESTIN, SP7. Endothelial cells: CD34. Periodontal tissues: POSTN. Msx1$^+$ regions: anti-tdTomato. Scale bars: top, 200 μm; middle and bottom, 50 μm.

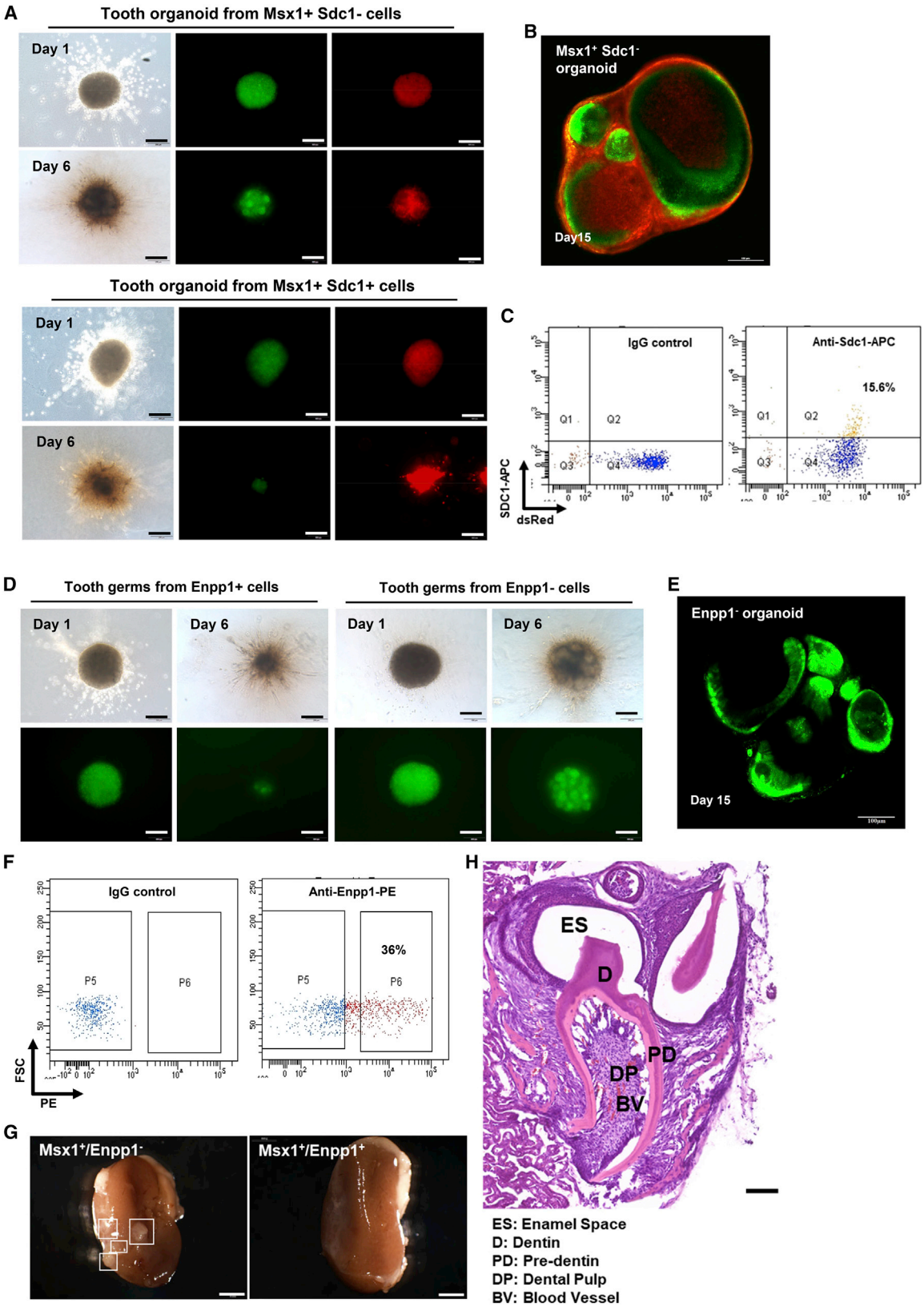

(legend on next page)

and expanded to form dental papilla at E13.5–E14.5 while disappearing from the mesenchymal region at P1 (Figure S9A). This suggested that the first group of dental papilla cells might be generated at E12.5. E12.5 scRNA-seq data identified 10 cell clusters, among which six were from mesenchymal lineage and four epithelial (Figure S9B). We then further analyzed the signature gene expression in the cell clusters (Figure S9C) and did pseudotime trajectory analysis of mesenchymal lineage using both Monocle2 and RNA velocity.[68] Monocle2 revealed that dental niche cells indeed were at an earlier progenitor state than dental papilla precursors (marked by *Lef1*, *Cxcl14*, *Tbx18*, and *Pantr1*) (Figure S10), an observation similar to our previous analysis using E14.5 mesenchymal cells (Figure S7). Moreover, RNA velocity revealed more details regarding the key cell composition contributing to dental papilla precursors. It was found that cluster 6 niche cells (marked by *Fxyd7*, *Pax9*, *Tfap2b*, and *Sox9*) seemed to play a central role in differentiating into both dental papilla precursors (cluster 2) and other niche cells (Figures 6A and S11). Immunostaining revealed that all the Sox9$^+$ niche cells were also Msx1$^+$ (tdTomato$^+$) (Figures 6B and S12). Msx1$^+$ Sox9$^+$ cells were first observed in the dental niche in E12.5, then surrounded the dental papilla by E14.5. At E15.5 these cells started to be detected in the dental papilla region, and a majority of dental papilla became Msx1$^+$Sox9$^+$ at E16.5. By E18.5 and P1, all the cells within the dental papilla region were Msx1$^+$ Sox9$^+$ (Figure 6B). CellChat analysis also found that dental niche cells (Msx1$^+$ Sox9$^+$ Enpp1$^-$) were the main cell population that communicated with dental papilla (Msx1$^+$ Sox9$^-$ Enpp1$^+$) and various dental epithelial cells (Figure S11B). These data suggested that the Msx1$^+$ Sox9$^+$ dental niche cells might represent a group of progenitors that migrated and replaced the original primordium during tooth morphogenesis.

Msx1$^+$Sox9$^+$ niche cells directly contributed to tooth morphogenesis

To evaluate the fate of Msx1$^+$Sox9$^+$ cells, we first confirmed that all the niche Sox9$^+$ cells were also Msx1$^+$ by both immunostaining (Figures S12A–S12C) and FACS analysis of transgenic animals from crossing the Sox9-EGFP[69] and Msx1-tdTomato mice (Figure S12D), which suggested that a single reporter lineage tracing model would be sufficient to track these cells. We then investigated whether Msx1$^+$ Sox9$^+$ cells directly contributed to tooth development *in vivo* by using the previously reported Sox9$^{IRES\text{-}CreERT2}$ mouse model[70] and LoxP-STOP-LoxP-tdTomato mice (ROSA26$^{LSL\text{-}tdTomato}$). Single labeling with tamoxifen was done at E11.5∼E12, and the labeled cells were analyzed at multiple points (E13.5–P1) (Figure 6C). While only a small fraction of tdTomato$^+$ cells were spotted in the dental niche regions at E13.5, tdTomato$^+$ cells were found surrounding the tooth germ at E14.5 and migrating into the dental papilla region at E16.5 and E18.5 (Figure 6C). By P1, large areas of tdTomato$^+$ cells were present in dental papilla regions of both maxillary and mandibular molars (Figure S13A). Moreover, quantitative analysis of adjacent tdTomato$^+$ cells indicated that more than 80% of Sox9$^+$ cells were in cell clusters, suggesting that they might have divided at least once during the migration (Figure S13B). Notably, most of the Sox9$^+$ cells might have divided more than twice, as about 60% of tdTomato$^+$ cell clusters contained more than four cells (Figure S13C). We also tried labeling by single injection at E13 (Figure S13D) and double labeling at E13 and E14 (Figure 6D), and in both cases, Sox9$^+$ cells were detected first in the niche regions at E15.5 and within the dental papilla at E18.5. In addition, we also isolated tooth germs for lineage tracing *in vitro* in the organoid culture (Figure 6E). 4-OHT was added for 24 h to label Sox9$^+$ cells, and tooth germs were further cultured for an additional 6 days. Indeed, many cells in the dental papilla became tdTomato$^+$, suggesting that the niche cells indeed migrated into the region (Figure 6E). To further confirm if dental niche cells were also directly involved in tooth germ reconstitution, tooth germs were dissociated into single cells and recombined *in vitro* before 4-OHT induction. Indeed, newly formed tooth germ-like structures with many tdTomato$^+$ cells in the dental papilla region could be observed within 10 days of culture (Figure 6F). Finally, to test if Sox9$^+$ niche cells would possess the tooth reconstitution capability, we used the Sox9-EGFP mice to isolate Sox9$^+$ cells from dental mesenchyme at E14.5 and E15.5 for tooth reconstitution (Figure S14A). Indeed, Sox9$^+$ cells from both stages were enriched with tooth induction capability, while none of the recombinants from Sox9$^-$ cells formed any tooth-like structures (Figures S14B and S14C). Moreover, the tooth-like structures from Sox9$^+$ recombinants exhibited normal anatomy (Figure S14D). Altogether, these data strongly supported that Msx1$^+$Sox9$^+$ dental niche cells directly contributed to the developing dental papilla *in vivo* and represented a previously unappreciated stem cell population that possessed tooth reconstitution capability.

Msx1$^+$Sox9$^+$ dental niche cells exhibited unique features and heterogeneity during tooth development

As mentioned earlier, niche cells migrated into the dental papilla region at around E15.5∼E16.5 (Figure 6B). To investigate the potential changes of these migrating cells, we compared the overall

Figure 5. Msx1$^+$Sdc1$^-$ niche cells promoted epithelium reorganization and long-term maintenance of tooth organoids

(A) Msx1$^+$Sdc1$^-$ niche cells promoted epithelium reorganization and survival during organoid culture. Representative organoids cultured for 6 days are shown. Scale bars: 200 μm. Msx1$^+$Sdc1$^-$, n = 16; Msx1$^+$Sdc1$^+$, n = 7.

(B) Representative image of tooth organoid cultured for 15 days in Msx1$^+$Sdc1$^-$ group. Msx1$^+$Sdc1$^+$ organoid did not survive. Scale bar: 100 μm.

(C) Msx1$^+$Sdc1$^+$ dental papilla cells could be regenerated from the reconstituted tooth organoid. The organoid was cultured for 6 days before analysis by anti-SDC1-APC staining. IgG: negative control.

(D) Msx1$^+$Enpp1$^-$ niche cells promoted epithelial reorganization and survival but not Msx1$^+$Enpp1$^+$ dental papilla cells. Msx1$^+$Enpp1$^-$, n = 12; Msx1$^+$Enpp1$^+$, n = 6. A representative image of organoids cultured for 6 days is shown. Scale bars: 200 μm.

(E) Representative image of tooth organoid cultured for 15 days in Msx1$^+$Enpp1$^-$ group. Scale bar: 100 μm.

(F) Msx1$^+$Enpp1$^+$ dental papilla cells could also be regenerated from the Msx1$^+$Enpp1$^-$ cell-reconstituted tooth germ organoid.

(G) Only Msx1$^+$Enpp1$^-$-reconstituted tooth germs could form tooth-like structures *in vivo*. The samples were harvested 4 weeks after transplantation. Scale: 2 mm.

(H) H&E staining confirmed the formation of tooth-like structures. Scale bars: 500 μm.

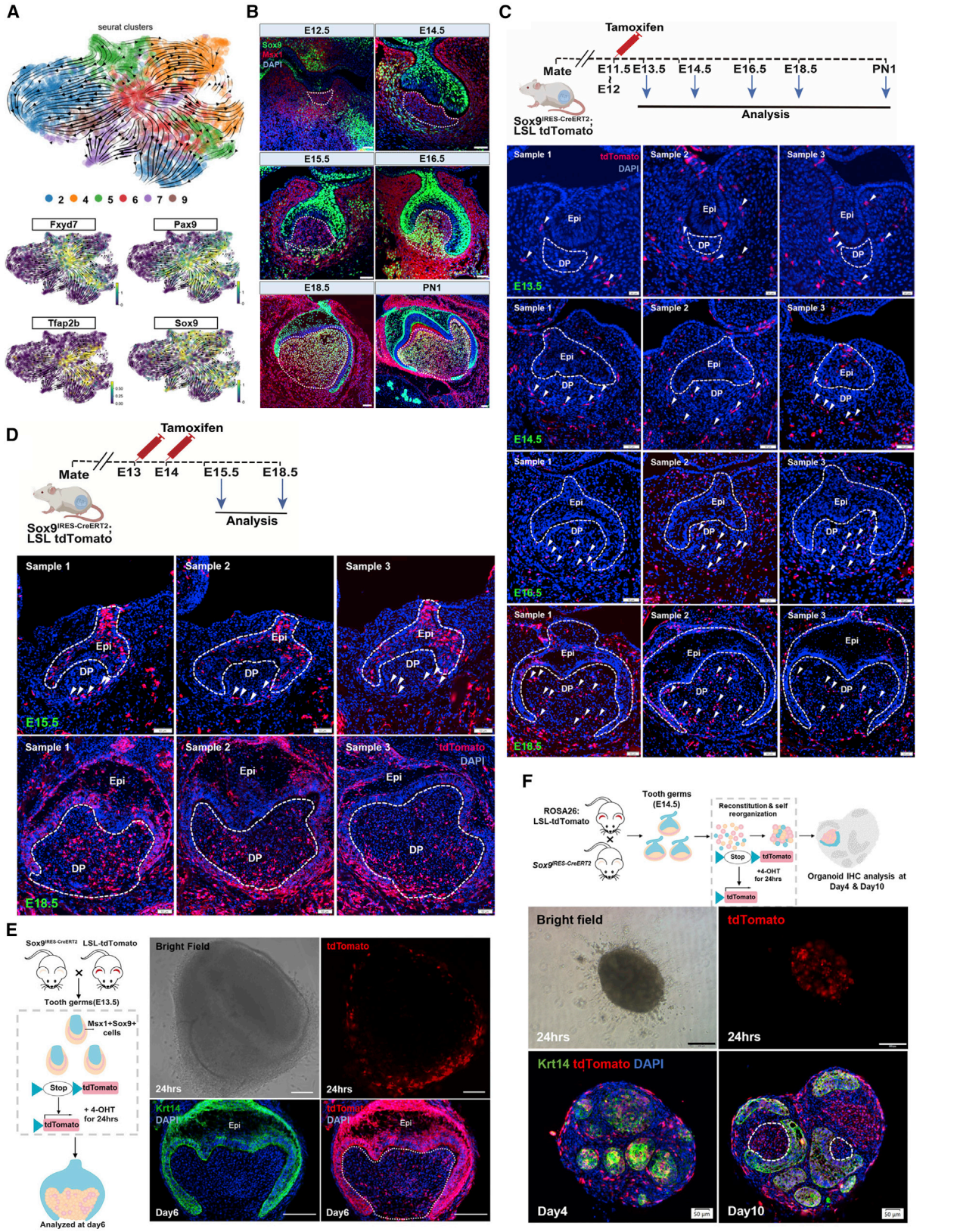

(legend on next page)

gene expression of TFs in Msx1$^+$Sox9$^+$ cells from E12.5, E14.5, and E16.5. Indeed, Msx1$^+$Sox9$^+$ cells from E16.5 showed activation of a set of unique TFs (Figure 7A), many of which were known regulators of tooth morphogenesis, such as *Creb3l1*,[71] *Runx1/Stat3*,[72,73] *Runx2*,[74,75] *Sp7*,[76] and *Irf8*,[77] etc. These data suggested that once the dental niche cells migrated into the dental papilla region, the gene network governing tooth morphogenesis might be activated. In addition, to evaluate the potential cellular heterogeneity, we also compared dental niche cells (Msx1$^+$ Sox9$^+$ Enpp1$^-$) vs. dental papilla (Msx1$^+$ Sox9$^-$ Enpp1$^+$) at E14.5 in their TF expression profile. Although dental papilla cells were relatively homogenous, considerable heterogeneity existed in the dental niche cell group (Figure 7B), warranting further investigation in these sub-groups. Altogether, our data indicated that the migrating dental niche cells would activate the tooth morphogenesis-associated gene network once entering the papilla region, and there were cell sub-groups within the niche that might have distinct functions.

DISCUSSION

In this study, we developed a dual-fluorescence model to track dental cells in mice and use it for scRNA-seq analysis, revealing the cellular dynamics during mouse molar development and molecular signatures of dental cell clusters. By combining spatial mapping with DistMap and tooth reconstitution using sorted cell populations, we discovered that niche cells were much more efficient to induce tooth formation than dental papilla cells, potentially by promoting the reorganization and survival of dental epithelium. Finally, through pseudotime trajectory analysis, lineage tracing *in vivo*, and organoid culture *in vitro*, we provided evidence for the direct contribution of Msx1$^+$Sox9$^+$ dental niche cells in molar development (Figure 7C).

The development and application of scRNA-seq have revolutionized the field of developmental biology. Recent work in mouse incisors also provided a rich resource on the cellular dynamics during incisor development[29,31] as well as neural crest-derived lineage diversification.[32] However, although molar development was believed to be more relevant to that of human teeth, the lack of precise cell labeling severely limited the study of mouse molars with scRNA-seq. By using reporter knockin mice, we were able to use FACS to isolate dental epithelium with copGFP and mesenchyme with tdTomato for downstream scRNA-seq analysis. Moreover, we showed that Pitx2$^+$ epithelial cells and Msx1$^+$ mesenchymal cells were sufficient to reconstitute a functional tooth germ, suggesting that these cells contained the essential information for inductive dental epithelial-mesenchymal interactions.

The construction of the virtual tooth model aimed to assist in further dissection of the key cell compositions in the developing teeth. Our tooth model was able to spatially map about 15,967 molar-expressed genes detected in scRNA-seq. Genes with unique restricted expression profiles were indeed identified. For example, *Sdc1* and *Enpp1* were specifically enriched in developing dental papilla, as confirmed by RNA-scope and IHF (Figure 3D), and previous ISH results could only suggest that *Enpp1* was a dental mesenchymal gene,[17] while *Sdc1* was present in both dental epithelium and mesenchyme.[78,79] Besides, several genes, such as *C1qtnf3*, *Cdkn1c*, and *Postn*, were found to be specifically expressed in the dental niche. Therefore, with the help of the virtual tooth model, we could characterize the spatial distribution of molar genes more clearly and accurately.

Finally, the discovery that the dental niche cells might be the main mediator of dental epithelial-mesenchymal interactions provided interesting insights regarding the cellular basis of such an important developmental process. Epithelial-mesenchymal interaction is the fundamental process that drives the morphogenesis of many mammalian organs. However, the cellular basis for such interaction was largely unknown. Especially in tooth development, although many molecular pathways and genes have been thoroughly investigated over the last 20 years, the exact cell population that drives the dental epithelial-mesenchymal interaction and its molecular identity are still elusive. Dental papilla cells were often assumed to play a critical role in this process and thus became the focus of previous research. It is worth noting that previous studies using lipophilic membrane stain had hinted that the development of dental papilla might require an additional influx of cells from the dental niche,[80] but those observations have not been further explored yet. In this study, through spatial mapping and functional validation, dental niche cells were found to play an important role in driving the epithelial-mesenchymal interacting process. These cells could induce tooth formation in clusters, promote reorganization and survival of the dental epithelium, and regenerate Msx1$^+$Sdc1$^+$ dental papilla cells. Lastly, lineage tracing *in vivo* confirmed that Msx1$^+$ Sox9$^+$ dental niche cells directly contributed to the dental papilla. These niche cells migrated into the dental papilla and become the main cell composition. Together, our data have identified a previously unappreciated role of dental niche cells in tooth formation and have provided novel insights on the critical cell composition that participates in tooth development, which may shed light on designing next-generation tooth bioengineering strategies to achieve the eventual goal of *de novo* tooth regeneration.

Figure 6. A group of Msx1$^+$Sox9$^+$ niche cells might be the origin of the dental papilla

(A) RNA velocity analysis suggested that dental niche cells from clusters 5 and 6 might be the origin of the dental papilla. Arrow indicates the projected flow of differentiation. Markers for cluster 6 niche cells: Fxyd7, Pax9, Tfap2b, and Sox9. Sox9 seemed to be shared by both group 5 and group 6 cells.

(B) Msx1$^+$ Sox9$^+$ niche cells seemed to gradually migrate and became a major part of dental papilla during tooth development. Frozen sections were immunostained with anti-Sox9. Msx1$^+$ regions: anti-tdTomato expression. Scale bar: 50 μm.

(C and D) Single and double labeling of lineage tracing *in vivo* confirmed the migration of Sox9$^+$ cells into dental papilla. Arrow indicates tdTomato$^+$ cells. Scale bar: 50 μm.

(E) Msx1$^+$ Sox9$^+$ niche cells migrated and directly contributed to dental papilla during tooth germ development. Krt14: dental epithelium marker. Scale bar: 100 μm.

(F) During tooth reconstitution, Msx1$^+$ Sox9$^+$ niche cells could also migrate and directly contributed to the dental papilla. Scale bar: 200 μm (top) and 50 μm (bottom).

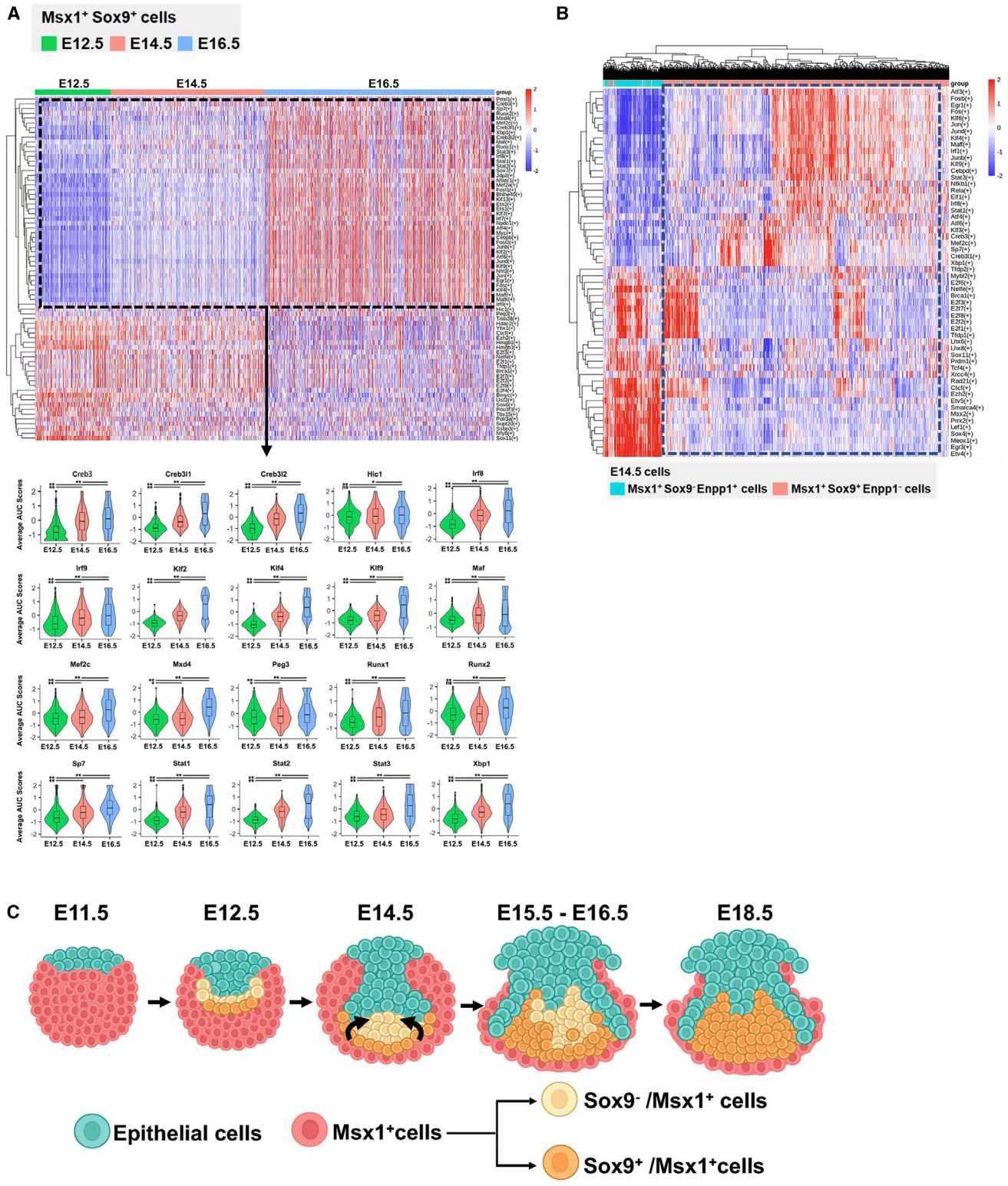

Figure 7. Msx1$^+$Sox9$^+$ dental niche cells exhibited unique features during molar development

(A) Activating differentiation network in dental niche cells at E16.5. The expression profile of TFs (transcription factors) in dental niche cells from E12.5, 14.5, and 16.5 were compared. When dental niche cells started migration into the dental papilla (E16.5), a set of differentiation-associated transcription factors were strongly activated. Statistics: t test by R package ggsignif. *$p < 0.01$; **$p < 0.001$. NS, not significant.

(B) Cellular heterogeneity could be observed in dental niche cells. E14.5 cells were used as an example.

(C) A model of mouse molar development with Msx1$^+$Sox9$^+$ dental niche cells.

Limitations of the study

Our work focused on the relationship between dental papilla and niche cells. One of the limitations was using only single-gene labeling for lineage tracing. A combination of both Cre and Dre systems would help to label niche cells more precisely. The spatial mapping by DistMap was also limited to E14.5 due to its reliance on published imaging data. Finally, the fate of the original dental primordium was not clear in this manuscript. We provided evidence that niche cells migrated into the papilla region, but what happened to the original cells there and their potential biological functions remain to be characterized.

STAR★METHODS

Detailed methods are provided in the online version of this paper and include the following:

- KEY RESOURCES TABLE
- RESOURCE AVAILABILITY
  - Lead contact
  - Materials availability
  - Data and code availability
- EXPERIMENTAL MODEL AND SUBJECT DETAILS
  - Mouse strains and animal care
- METHOD DETAILS
  - Tooth germ isolation and single-cell preparation
  - Tooth germ reconstitution *in vitro*
  - Renal capsule transplantation
  - Micro-computed tomography (Micro-CT) analysis
  - Tissue sections and histological analysis
  - Immunofluorescence for tissue sections
  - Fluorescence-activated cell sorting (FACS)
  - Culture of the tooth germ organoid
  - Single-cell preparation and scRNA sequencing
  - Lineage tracing of $Sox9^{+}$ cells
  - Quantitative PCR
  - Processing of scRNA-seq raw sequencing data
  - Reduction, clustering, and identification of differentially expressed genes
  - Parameters for processing scRNA-seq data
  - Spatial mapping of gene expression
  - Molar data integration
  - Pseudotemporal trajectory analysis
  - CytoTRACE and cellRank analysis
  - pySCENIC analysis
  - CellChat receptor-ligand analysis
- QUANTIFICATION AND STATISTICAL ANALYSIS

SUPPLEMENTAL INFORMATION

Supplemental information can be found online at https://doi.org/10.1016/j.celrep.2022.111737.

ACKNOWLEDGMENTS

We thank Han Kang from Core Facilities in the College of Life Sciences for his technical assistance, Prof. Ting Chen from the National Institute of Biological Sciences (Beijing) for her kind gift of the Sox9-CreERT2 mice, and Prof. Jia Yu from the Institute of Basic Medical Sciences, Chinese Academy of Medical Sciences for his instructions on bioinformatic analysis. This work was funded by the National Key Research and Development Program of China (2021YFA1100601, 2017YFA0104801), National Natural Science Foundation of China (32071455), Sichuan Science & Technology Program (2021ZDZX0010), SCU grant (020SCUNL109), and the Fundamental Research Funds for the Central Universities (SCU2019D013).

AUTHOR CONTRIBUTIONS

Conceiving: Z.L., H.H., Y.D., K.W., and H.F. Most of the experiments: Y.D. and H.H. Bioinformatic analysis: K.W., H.F., and F.K. Organoid: H.H., Y.D., and Z.Z. Micro-CT: F.H. and Y.L. Animal work and sorting: Y.L., H.H., B.Z., H.Z., Z.Z., Y.Y., and J.X. Oversight and data interpretation: W.T., H.C., and Z.L. Writing: Z.L., H.H., Y.D., K.W., and H.F. wrote the manuscript. All authors have seen and approved the final version of the paper.

DECLARATION OF INTERESTS

The authors declare that they have no competing interests.

Received: July 25, 2022
Revised: August 10, 2022
Accepted: November 7, 2022
Published: December 6, 2022

REFERENCES

1. Xuan, K., Li, B., Guo, H., Sun, W., Kou, X., He, X., Zhang, Y., Sun, J., Liu, A., Liao, L., et al. (2018). Deciduous autologous tooth stem cells regenerate dental pulp after implantation into injured teeth. Sci. Transl. Med. *10*, eaaf3227. https://doi.org/10.1126/scitranslmed.aaf3227.
2. Sonoyama, W., Liu, Y., Yamaza, T., Tuan, R.S., Wang, S., Shi, S., and Huang, G.T.J. (2008). Characterization of the apical papilla and its residing stem cells from human immature permanent teeth: a pilot study. J. Endod. *34*, 166–171. https://doi.org/10.1016/j.joen.2007.11.021.
3. Miura, M., Gronthos, S., Zhao, M., Lu, B., Fisher, L.W., Robey, P.G., and Shi, S. (2003). SHED: stem cells from human exfoliated deciduous teeth. Proc. Natl. Acad. Sci. USA *100*, 5807–5812. https://doi.org/10.1073/pnas.0937635100.
4. Morsczeck, C., Götz, W., Schierholz, J., Zeilhofer, F., Kühn, U., Möhl, C., Sippel, C., and Hoffmann, K.H. (2005). Isolation of precursor cells (PCs) from human dental follicle of wisdom teeth. Matrix Biol. *24*, 155–165. https://doi.org/10.1016/j.matbio.2004.12.004.
5. Seo, B.M., Miura, M., Gronthos, S., Mark Bartold, P., Batouli, S., Brahim, J., Young, M., Gehron Robey, P., Wang, C.Y., and Shi, S. (2004). Investigation of multipotent postnatal stem cells from human periodontal ligament. Lancet *364*, 149–155. https://doi.org/10.1016/s0140-6736(04)16627-0.
6. Gronthos, S., Mankani, M., Brahim, J., Robey, P.G., and Shi, S. (2000). Postnatal human dental pulp stem cells (DPSCs) in vitro and in vivo. Proc. Natl. Acad. Sci. USA *97*, 13625–13630. https://doi.org/10.1073/pnas.240309797.
7. Chen, H., Fu, H., Wu, X., Duan, Y., Zhang, S., Hu, H., Liao, Y., Wang, T., Yang, Y., Chen, G., et al. (2020). Regeneration of pulpo-dentinal-like complex by a group of unique multipotent CD24a(+) stem cells. Sci. Adv. *6*, eaay1514. https://doi.org/10.1126/sciadv.aay1514.
8. Zhang, W., and Yelick, P.C. (2021). Tooth repair and regeneration: potential of dental stem cells. Trends Mol. Med. *27*, 501–511. https://doi.org/10.1016/j.molmed.2021.02.005.
9. Yelick, P.C., and Sharpe, P.T. (2019). Tooth bioengineering and regenerative dentistry. J. Dent. Res. *98*, 1173–1182. https://doi.org/10.1177/0022034519861903.
10. Nakao, K., Morita, R., Saji, Y., Ishida, K., Tomita, Y., Ogawa, M., Saitoh, M., Tomooka, Y., and Tsuji, T. (2007). The development of a bioengineered

organ germ method. Nat. Methods *4*, 227–230. https://doi.org/10.1038/nmeth1012.

11. Mina, M., and Kollar, E.J. (1987). The induction of odontogenesis in non-dental mesenchyme combined with early murine mandibular arch epithelium. Arch. Oral Biol. *32*, 123–127. https://doi.org/10.1016/0003-9969(87)90055-0.
12. Cai, J., Zhang, Y., Liu, P., Chen, S., Wu, X., Sun, Y., Li, A., Huang, K., Luo, R., Wang, L., et al. (2013). Generation of tooth-like structures from integration-free human urine induced pluripotent stem cells. Cell Regen. *2*, 6. https://doi.org/10.1186/2045-9769-2-6.
13. Cai, J., Cho, S.W., Kim, J.Y., Lee, M.J., Cha, Y.G., and Jung, H.S. (2007). Patterning the size and number of tooth and its cusps. Dev. Biol. *304*, 499–507. https://doi.org/10.1016/j.ydbio.2007.01.002.
14. Lin, C., Ruan, N., Li, L., Chen, Y., Hu, X., Chen, Y., Hu, X., and Zhang, Y. (2022). FGF8-mediated signaling regulates tooth developmental pace during odontogenesis. J Genet Genomics *49*, 40–53. https://doi.org/10.1016/j.jgg.2021.08.009.
15. Tucker, A., and Sharpe, P. (2004). The cutting-edge of mammalian development; how the embryo makes teeth. Nat. Rev. Genet. *5*, 499–508. https://doi.org/10.1038/nrg1380.
16. Vainio, S., Karavanova, I., Jowett, A., and Thesleff, I. (1993). Identification of BMP-4 as a signal mediating secondary induction between epithelial and mesenchymal tissues during early tooth development. Cell *75*, 45–58.
17. James, M.J., Järvinen, E., Wang, X.P., and Thesleff, I. (2006). Different roles of Runx2 during early neural crest-derived bone and tooth development. J. Bone Miner. Res. *21*, 1034–1044. https://doi.org/10.1359/jbmr.060413.
18. Hardcastle, Z., Mo, R., Hui, C.C., and Sharpe, P.T. (1998). The Shh signalling pathway in tooth development: defects in Gli2 and Gli3 mutants. Development *125*, 2803–2811. https://doi.org/10.1242/dev.125.15.2803.
19. Zhang, Y.D., Chen, Z., Song, Y.Q., Liu, C., and Chen, Y.P. (2005). Making a tooth: growth factors, transcription factors, and stem cells. Cell Res. *15*, 301–316. https://doi.org/10.1038/sj.cr.7290299.
20. Balic, A. (2019). Concise review: cellular and molecular mechanisms regulation of tooth initiation. Stem Cell. *37*, 26–32. https://doi.org/10.1002/stem.2917.
21. Ahtiainen, L., Uski, I., Thesleff, I., and Mikkola, M.L. (2016). Early epithelial signaling center governs tooth budding morphogenesis. J. Cell Biol. *214*, 753–767. https://doi.org/10.1083/jcb.201512074.
22. Stuart, T., and Satija, R. (2019). Integrative single-cell analysis. Nat. Rev. Genet. *20*, 257–272. https://doi.org/10.1038/s41576-019-0093-7.
23. Grün, D., Lyubimova, A., Kester, L., Wiebrands, K., Basak, O., Sasaki, N., Clevers, H., and van Oudenaarden, A. (2015). Single-cell messenger RNA sequencing reveals rare intestinal cell types. Nature *525*, 251–255. https://doi.org/10.1038/nature14966.
24. Barruet, E., Garcia, S.M., Striedinger, K., Wu, J., Lee, S., Byrnes, L., Wong, A., Xuefeng, S., Tamaki, S., Brack, A.S., and Pomerantz, J.H. (2020). Functionally heterogeneous human satellite cells identified by single cell RNA sequencing. Elife *9*, e51576. https://doi.org/10.7554/eLife.51576.
25. Nabhan, A.N., Brownfield, D.G., Harbury, P.B., Krasnow, M.A., and Desai, T.J. (2018). Single-cell Wnt signaling niches maintain stemness of alveolar type 2 cells. Science *359*, 1118–1123. https://doi.org/10.1126/science.aam6603.
26. Giladi, A., Paul, F., Herzog, Y., Lubling, Y., Weiner, A., Yofe, I., Jaitin, D., Cabezas-Wallscheid, N., Dress, R., Ginhoux, F., et al. (2018). Single-cell characterization of haematopoietic progenitors and their trajectories in homeostasis and perturbed haematopoiesis. Nat. Cell Biol. *20*, 836–846. https://doi.org/10.1038/s41556-018-0121-4.
27. Patil, V.S., Madrigal, A., Schmiedel, B.J., Clarke, J., O'Rourke, P., de Silva, A.D., Harris, E., Peters, B., Seumois, G., Weiskopf, D., et al. (2018). Precursors of human CD4(+) cytotoxic T lymphocytes identified by single-cell transcriptome analysis. Sci. Immunol. *3*, eaan8664. https://doi.org/10.1126/sciimmunol.aan8664.
28. Zeng, Y., Liu, C., Gong, Y., Bai, Z., Hou, S., He, J., Bian, Z., Li, Z., Ni, Y., Yan, J., et al. (2019). Single-cell RNA sequencing resolves spatiotemporal development of pre-thymic lymphoid progenitors and thymus organogenesis in human embryos. Immunity *51*, 930–948.e6. https://doi.org/10.1016/j.immuni.2019.09.008.
29. Sharir, A., Marangoni, P., Zilionis, R., Wan, M., Wald, T., Hu, J.K., Kawaguchi, K., Castillo-Azofeifa, D., Epstein, L., Harrington, K., et al. (2019). A large pool of actively cycling progenitors orchestrates self-renewal and injury repair of an ectodermal appendage. Nat. Cell Biol. *21*, 1102–1112. https://doi.org/10.1038/s41556-019-0378-2.
30. Krivanek, J., Soldatov, R.A., Kastriti, M.E., Chontorotzea, T., Herdina, A.N., Petersen, J., Szarowska, B., Landova, M., Matejova, V.K., Holla, L.I., et al. (2020). Dental cell type atlas reveals stem and differentiated cell types in mouse and human teeth. Nat. Commun. *11*, 4816. https://doi.org/10.1038/s41467-020-18512-7.
31. Chiba, Y., Saito, K., Martin, D., Boger, E.T., Rhodes, C., Yoshizaki, K., Nakamura, T., Yamada, A., Morell, R.J., Yamada, Y., and Fukumoto, S. (2020). Single-cell RNA-sequencing from mouse incisor reveals dental epithelial cell-type specific genes. Front. Cell Dev. Biol. *8*, 841. https://doi.org/10.3389/fcell.2020.00841.
32. Jing, J., Feng, J., Yuan, Y., Guo, T., Lei, J., Pei, F., Ho, T.V., and Chai, Y. (2022). Spatiotemporal single-cell regulatory atlas reveals neural crest lineage diversification and cellular function during tooth morphogenesis. Nat. Commun. *13*, 4803. https://doi.org/10.1038/s41467-022-32490-y.
33. Karaiskos, N., Wahle, P., Alles, J., Boltengagen, A., Ayoub, S., Kipar, C., Kocks, C., Rajewsky, N., and Zinzen, R.P. (2017). The Drosophila embryo at single-cell transcriptome resolution. Science *358*, 194–199. https://doi.org/10.1126/science.aan3235.
34. Balic, A., and Thesleff, I. (2015). Tissue interactions regulating tooth development and renewal. Curr. Top. Dev. Biol. *115*, 157–186. https://doi.org/10.1016/bs.ctdb.2015.07.006.
35. Szeto, D.P., Rodriguez-Esteban, C., Ryan, A.K., O'Connell, S.M., Liu, F., Kioussi, C., Gleiberman, A.S., Izpisúa-Belmonte, J.C., and Rosenfeld, M.G. (1999). Role of the Bicoid-related homeodomain factor Pitx1 in specifying hindlimb morphogenesis and pituitary development. Genes Dev. *13*, 484–494. https://doi.org/10.1101/gad.13.4.484.
36. Suh, H., Gage, P.J., Drouin, J., and Camper, S.A. (2002). Pitx2 is required at multiple stages of pituitary organogenesis: pituitary primordium formation and cell specification. Development (Cambridge, England) *129*, 329–337. https://doi.org/10.1242/dev.129.2.329.
37. Gage, P.J., Qian, M., Wu, D., and Rosenberg, K.I. (2008). The canonical Wnt signaling antagonist DKK2 is an essential effector of PITX2 function during normal eye development. Dev. Biol. *317*, 310–324. https://doi.org/10.1016/j.ydbio.2008.02.030.
38. Berry, F.B., Lines, M.A., Oas, J.M., Footz, T., Underhill, D.A., Gage, P.J., and Walter, M.A. (2006). Functional interactions between FOXC1 and PITX2 underlie the sensitivity to FOXC1 gene dose in Axenfeld-Rieger syndrome and anterior segment dysgenesis. Hum. Mol. Genet. *15*, 905–919. https://doi.org/10.1093/hmg/ddl008.
39. Bélanger, M.C., Robert, B., and Cayouette, M. (2017). Msx1-Positive progenitors in the retinal ciliary margin give rise to both neural and non-neural progenies in mammals. Dev. Cell *40*, 137–150. https://doi.org/10.1016/j.devcel.2016.11.020.
40. Lu, C.H., Rincón-Limas, D.E., and Botas, J. (2000). Conserved overlapping and reciprocal expression of msh/Msx1 and apterous/Lhx2 in Drosophila and mice. Mech. Dev. *99*, 177–181. https://doi.org/10.1016/s0925-4773(00)00479-2.
41. Coudert, A.E., Pibouin, L., Vi-Fane, B., Thomas, B.L., Macdougall, M., Choudhury, A., Robert, B., Sharpe, P.T., Berdal, A., and Lezot, F. (2005). Expression and regulation of the Msx1 natural antisense transcript during development. Nucleic Acids Res. *33*, 5208–5218. https://doi.org/10.1093/nar/gki831.

42. Rothová, M., Feng, J., Sharpe, P.T., Peterková, R., and Tucker, A.S. (2011). Contribution of mesoderm to the developing dental papilla. Int. J. Dev. Biol. *55*, 59–64. https://doi.org/10.1387/ijdb.103083mr.

43. Nakatomi, M., Quispe-Salcedo, A., Sakaguchi, M., Ida-Yonemochi, H., Okano, H., and Ohshima, H. (2018). Nestin expression is differently regulated between odontoblasts and the subodontoblastic layer in mice. Histochem. Cell Biol. *149*, 383–391. https://doi.org/10.1007/s00418-018-1651-3.

44. Ono, W., Sakagami, N., Nishimori, S., Ono, N., and Kronenberg, H.M. (2016). Parathyroid hormone receptor signalling in osterix-expressing mesenchymal progenitors is essential for tooth root formation. Nat. Commun. *7*, 11277. https://doi.org/10.1038/ncomms11277.

45. Wang, Y., Cox, M.K., Coricor, G., MacDougall, M., and Serra, R. (2013). Inactivation of Tgfbr2 in Osterix-Cre expressing dental mesenchyme disrupts molar root formation. Dev. Biol. *382*, 27–37. https://doi.org/10.1016/j.ydbio.2013.08.003.

46. Mitsiadis, T.A., Chéraud, Y., Sharpe, P., and Fontaine-Pérus, J. (2003). Development of teeth in chick embryos after mouse neural crest transplantations. Proc. Natl. Acad. Sci. USA *100*, 6541–6545. https://doi.org/10.1073/pnas.1137104100.

47. Robinson, C., Brookes, S.J., Shore, R.C., and Kirkham, J. (1998). The developing enamel matrix: nature and function. Eur. J. Oral Sci. *106*, 282–291. https://doi.org/10.1111/j.1600-0722.1998.tb02188.x.

48. Brookes, S.J., Robinson, C., Kirkham, J., and Bonass, W.A. (1995). Biochemistry and molecular biology of amelogenin proteins of developing dental enamel. Arch. Oral Biol. *40*, 1–14. https://doi.org/10.1016/0003-9969(94)00135-x.

49. Horiuchi, K., Amizuka, N., Takeshita, S., Takamatsu, H., Katsuura, M., Ozawa, H., Toyama, Y., Bonewald, L.F., and Kudo, A. (1999). Identification and characterization of a novel protein, periostin, with restricted expression to periosteum and periodontal ligament and increased expression by transforming growth factor beta. J. Bone Miner. Res. *14*, 1239–1249. https://doi.org/10.1359/jbmr.1999.14.7.1239.

50. Trubiani, O., Tripodi, D., Delle Fratte, T., Caputi, S., and Di Primio, R. (2003). Human dental pulp vasculogenesis evaluated by CD34 antigen expression and morphological arrangement. J. Dent. Res. *82*, 742–747. https://doi.org/10.1177/154405910308200916.

51. Qiu, X., Mao, Q., Tang, Y., Wang, L., Chawla, R., Pliner, H.A., and Trapnell, C. (2017). Reversed graph embedding resolves complex single-cell trajectories. Nat. Methods *14*, 979–982. https://doi.org/10.1038/nmeth.4402.

52. Kettunen, P., Laurikkala, J., Itäranta, P., Vainio, S., Itoh, N., and Thesleff, I. (2000). Associations of FGF-3 and FGF-10 with signaling networks regulating tooth morphogenesis. Dev. Dynam. *219*, 322–332, an official publication of the American Association of Anatomists. https://doi.org/10.1002/1097-0177.

53. Zhang, J., Zheng, M., Eipper, B.A., and Pintar, J.E. (1997). Embryonic and uterine expression patterns of peptidylglycine alpha-amidating monooxygenase transcripts suggest a widespread role for amidated peptides in development. Dev. Biol. *192*, 375–391. https://doi.org/10.1006/dbio.1997.8750.

54. Jin, S., Guerrero-Juarez, C.F., Zhang, L., Chang, I., Ramos, R., Kuan, C.H., Myung, P., Plikus, M.V., and Nie, Q. (2021). Inference and analysis of cell-cell communication using CellChat. Nat. Commun. *12*, 1088. https://doi.org/10.1038/s41467-021-21246-9.

55. Vercauteren Drubbel, A., Pirard, S., Kin, S., Dassy, B., Lefort, A., Libert, F., Nomura, S., and Beck, B. (2021). Reactivation of the Hedgehog pathway in esophageal progenitors turns on an embryonic-like program to initiate columnar metaplasia. Cell Stem Cell *28*, 1411–1427.e7. https://doi.org/10.1016/j.stem.2021.03.019.

56. Cao, E.Y., Ouyang, J.F., and Rackham, O.J.L. (2020). GeneSwitches: ordering gene expression and functional events in single-cell experiments. Bioinformatics *36*, 3273–3275. https://doi.org/10.1093/bioinformatics/btaa099.

57. Liu, Z., Li, C., Xu, J., Lan, Y., Liu, H., Li, X., Maire, P., Wang, X., and Jiang, R. (2019). Crucial and overlapping roles of Six1 and Six2 in craniofacial development. J. Dent. Res. *98*, 572–579. https://doi.org/10.1177/0022034519835204.

58. Zhao, Y., Guo, Y.J., Tomac, A.C., Taylor, N.R., Grinberg, A., Lee, E.J., Huang, S., and Westphal, H. (1999). Isolated cleft palate in mice with a targeted mutation of the LIM homeobox gene lhx8. Proc. Natl. Acad. Sci. USA *96*, 15002–15006. https://doi.org/10.1073/pnas.96.26.15002.

59. Soldatov, R., Kaucka, M., Kastriti, M.E., Petersen, J., Chontorotzea, T., Englmaier, L., Akkuratova, N., Yang, Y., Häring, M., Dyachuk, V., et al. (2019). Spatiotemporal structure of cell fate decisions in murine neural crest. Science *364*, eaas9536. https://doi.org/10.1126/science.aas9536.

60. Satokata, I., Ma, L., Ohshima, H., Bei, M., Woo, I., Nishizawa, K., Maeda, T., Takano, Y., Uchiyama, M., Heaney, S., et al. (2000). Msx2 deficiency in mice causes pleiotropic defects in bone growth and ectodermal organ formation. Nat. Genet. *24*, 391–395. https://doi.org/10.1038/74231.

61. Zheng, L., Iohara, K., Ishikawa, M., Into, T., Takano-Yamamoto, T., Matsushita, K., and Nakashima, M. (2007). Runx3 negatively regulates Osterix expression in dental pulp cells. Biochem. J. *405*, 69–75. https://doi.org/10.1042/bj20070104.

62. Descroix, V., Kato, S., Lézot, F., and Berdal, A. (2010). Physiopathology of dental rickets in vitamin D receptor-ablated mice. J. Dent. Res. *89*, 1427–1432. https://doi.org/10.1177/0022034510379603.

63. Chen, Z., Wu, W., Zheng, C., Lan, Y., Xie, H., and Xie, Z. (2022). KLF6 facilitates differentiation of odontoblasts through modulating the expression of P21 in vitro. Int. J. Oral Sci. *14*, 20. https://doi.org/10.1038/s41368-022-00172-6.

64. Felthaus, O., Gosau, M., Klein, S., Prantl, L., Reichert, T.E., Schmalz, G., and Morsczeck, C. (2014). Dexamethasone-related osteogenic differentiation of dental follicle cells depends on ZBTB16 but not Runx2. Cell Tissue Res. *357*, 695–705. https://doi.org/10.1007/s00441-014-1891-z.

65. Gulati, G.S., Sikandar, S.S., Wesche, D.J., Manjunath, A., Bharadwaj, A., Berger, M.J., Ilagan, F., Kuo, A.H., Hsieh, R.W., Cai, S., et al. (2020). Single-cell transcriptional diversity is a hallmark of developmental potential. Science *367*, 405–411. https://doi.org/10.1126/science.aax0249.

66. Lange, M., Bergen, V., Klein, M., Setty, M., Reuter, B., Bakhti, M., Lickert, H., Ansari, M., Schniering, J., Schiller, H.B., et al. (2022). CellRank for directed single-cell fate mapping. Nat. Methods *19*, 159–170. https://doi.org/10.1038/s41592-021-01346-6.

67. Zhang, F., Li, X., and Tian, W. (2020). Unsupervised inference of developmental directions for single cells using VECTOR. Cell Rep. *32*, 108069. https://doi.org/10.1016/j.celrep.2020.108069.

68. La Manno, G., Soldatov, R., Zeisel, A., Braun, E., Hochgerner, H., Petukhov, V., Lidschreiber, K., Kastriti, M.E., Lönnerberg, P., Furlan, A., et al. (2018). RNA velocity of single cells. Nature *560*, 494–498. https://doi.org/10.1038/s41586-018-0414-6.

69. Chan, H.Y., V, S., Xing, X., Kraus, P., Yap, S.P., Ng, P., Lim, S.L., and Lufkin, T. (2011). Comparison of IRES and F2A-based locus-specific multicistronic expression in stable mouse lines. PLoS One *6*, e28885. https://doi.org/10.1371/journal.pone.0028885.

70. Xu, Z., Wang, W., Jiang, K., Yu, Z., Huang, H., Wang, F., Zhou, B., and Chen, T. (2015). Embryonic attenuated Wnt/β-catenin signaling defines niche location and long-term stem cell fate in hair follicle. Elife *4*, e10567. https://doi.org/10.7554/eLife.10567.

71. Andersson, K., Malmgren, B., Åström, E., Nordgren, A., Taylan, F., and Dahllöf, G. (2020). Mutations in COL1A1/A2 and CREB3L1 are associated with oligodontia in osteogenesis imperfecta. Orphanet J. Rare Dis. *15*, 80. https://doi.org/10.1186/s13023-020-01361-4.

72. Sarper, S.E., Inubushi, T., Kurosaka, H., Ono Minagi, H., Kuremoto, K.I., Sakai, T., Taniuchi, I., and Yamashiro, T. (2018). Runx1-Stat3 signaling regulates the epithelial stem cells in continuously growing incisors. Sci. Rep. *8*, 10906. https://doi.org/10.1038/s41598-018-29317-6.

73. Yamashiro, T., Aberg, T., Levanon, D., Groner, Y., and Thesleff, I. (2002). Expression of Runx1, -2 and -3 during tooth, palate and craniofacial bone development. Mech. Dev. *119*, S107–S110. https://doi.org/10.1016/s0925-4773(03)00101-1.

74. Wen, Q., Jing, J., Han, X., Feng, J., Yuan, Y., Ma, Y., Chen, S., Ho, T.V., and Chai, Y. (2020). Runx2 regulates mouse tooth root development via activation of WNT inhibitor NOTUM. J. Bone Miner. Res. *35*, 2252–2264. https://doi.org/10.1002/jbmr.4120.

75. Aberg, T., Wang, X.P., Kim, J.H., Yamashiro, T., Bei, M., Rice, R., Ryoo, H.M., and Thesleff, I. (2004). Runx2 mediates FGF signaling from epithelium to mesenchyme during tooth morphogenesis. Dev. Biol. *270*, 76–93. https://doi.org/10.1016/j.ydbio.2004.02.012.

76. Bae, J.M., Clarke, J.C., Rashid, H., Adhami, M.D., McCullough, K., Scott, J.S., Chen, H., Sinha, K.M., de Crombrugghe, B., and Javed, A. (2018). Specificity protein 7 is required for proliferation and differentiation of ameloblasts and odontoblasts. J. Bone Miner. Res. *33*, 1126–1140. https://doi.org/10.1002/jbmr.3401.

77. Thumbigere-Math, V., Foster, B.L., Bachu, M., Yoshii, H., Brooks, S.R., Coulter, A., Chavez, M.B., Togi, S., Neely, A.L., Deng, Z., et al. (2019). Inactivating mutation in IRF8 promotes osteoclast transcriptional programs and increases susceptibility to tooth root resorption. J. Bone Miner. Res. *34*, 1155–1168. https://doi.org/10.1002/jbmr.3690.

78. Chen, Y., Bei, M., Woo, I., Satokata, I., and Maas, R. (1996). Msx1 controls inductive signaling in mammalian tooth morphogenesis. Development *122*, 3035–3044. https://doi.org/10.1242/dev.122.10.3035.

79. Thesleff, I., Vaahtokari, A., Vainio, S., and Jowett, A. (1996). Molecular mechanisms of cell and tissue interactions during early tooth development. Anat. Rec. *245*, 151–161. https://doi.org/10.1002/(sici)1097-0185.

80. Rothová, M., Peterková, R., and Tucker, A.S. (2012). Fate map of the dental mesenchyme: dynamic development of the dental papilla and follicle. Dev. Biol. *366*, 244–254. https://doi.org/10.1016/j.ydbio.2012.03.018.

STAR★METHODS

KEY RESOURCES TABLE

REAGENT or RESOURCE	SOURCE	IDENTIFIER
Antibodies		
Rabbit polyclonal anti-TurboGFP	ThermoFisher	Cat# PA5-22688; RRID:AB_2540616
Goat polyclonal anti-tdTomato	SICGEN	Cat# AB8181; RRID: AB_2722750
Rabbit polyclonal anti-Nestin	Huabio	Cat# R1510-19
Rabbit recombinant monoclonal anti-Sp7	Abcam	Cat# ab209484; RRID: AB_2892207
Rabbit polyclonal Anti-AMGN	Santa Cruz Biotechnology	Cat# sc-32892; RRID: AB_2226455
Rabbit polyclonal anti-AMBN	Santa Cruz Biotechnology	Cat# sc-50534; RRID:AB_2226393
Rabbit monoclonal anti-Cd34	Huabio	Cat# ET1606-11; RRID:AB_2924309
Rabbit monoclonal anti-Postn	Abcam	Cat# ab215199; RRID:AB_2924310
APC anti-mouse CD138	Biolegend	Cat#142505; RRID:AB_10960141
Rabbit monoclonal anti-p57 Kip2	Abcam	Cat# ab75974; RRID:AB_1310535
Rabbit monoclonal anti-Runx2	Huabio	Cat# ET1612-47; RRID:AB_2924311
Rabbit monoclonal anti-Sox9	Huabio	Cat# ET1611-56; RRID:AB_2924312
Chicken polyclonal anti-Krt14	Biolegend	Cat#906004; RRID:AB_2616962
Rabbit IgG	Abcam	Cat# ab172730; RRID:AB_2687931
Goat IgG	ThermoFisher	Cat# 31245; RRID:AB_10959406
Alexa fluor-647 rat IgG2a, κ isotype ctrl antibody	Biolegend	Cat#400526; RRID:AB_2864284
Chicken IgY	Aveslab	Cat# N-1010; RRID:AB_2313532
Alexa fluor-568 donkey anti goat	ThermoFisher	Cat #A11057; RRID:AB_142581
Alexa fluor-488 donkey anti rabbit	ThermoFisher	Cat# A21206; RRID:AB_2535792
Alexa fluor-647 donkey anti rabbit	ThermoFisher	Cat# A31573; RRID:AB_2536183
Alexa fluor-488 goat anti chicken	ThermoFisher	Cat# A11039; RRID:AB_142924
Critical commercial assays		
C1qtnf3 RNAscope	ACDbio	Cat#531451
Enpp1 RNAscope	ACDbio	Cat#441191
Opal 520 Regent	Asbio	Cat# ASOP520
Opal 690 Regent	Asbio	Cat# ASOP690
Deposited data		
Raw and analyzed data of Single RNA-seq	This paper	GEO: GSE162413
Tooth DistMap analysis model and data	This paper	https://github.com/victorwang123/toothatlas
Experimental models: Organisms/strains		
Mouse: C57BL/6-Pitx2-P2A-copGFP	This paper	N/A
Mouse: C57BL/6-Msx1-P2A-tdTomato	This paper	N/A
Mouse: C57BL/6-Sox9 $^{cre-ERT2}$/Tchn	National Institute of Biological Sciences in China	N/A
Mouse: C57BL/6-B6; 129S4-Sox9 $^{tm1.1Tlu}$/J	The Jackson Laboratory	Stock No: 030137; RRID: IMSR_JAX:030137
Mouse: C57BL/6-Gt(ROSA) 26Sortm1$^{(CAG-LSL-tdTomato)}$/Bcgen	Biocytogen	Stock No: 110148
Oligonucleotides		
Primers	This paper	Table S1
Software and algorithms		
ImageJ	https://imagej.nih.gov/ij/	RRID:SCR_003070
CellChat	https://github.com/sqjin/CellChat	RRID:SCR_021946

(*Continued on next page*)

Continued

REAGENT or RESOURCE	SOURCE	IDENTIFIER
SCIGA	https://github.com/sciensic/SCIGA	RRID:SCR_021002
Seurat	https://satijalab.org/seurat/get_started.html	RRID:SCR_016341
Scrublet	https://github.com/AllonKleinLab/scrublet	RRID:SCR_018098
DistMap	http://code.google.com/p/distmap/	RRID:SCR_005473
Monocle2	http://cole-trapnell-lab.github.io/monocle-release/docs/	RRID:SCR_016339
CytoTrace	https://cytotrace.stanford.edu/	RRID:SCR_022828
CellRank	https://cellrank.readthedocs.io/en/stable/	RRID:SCR_022827
GeneSwitches	https://geneswitches.ddnetbio.com	RRID:SCR_022826
pySCENIC	http://scenic.aertslab.org	RRID:SCR_017247
ShinyCell	https://github.com/SGDDNB/ShinyCell	RRID: SCR_022756

RESOURCE AVAILABILITY

Lead contact

Further information and requests for resources and reagents should be directed to Zhonghan Li (Zhonghan.Li@scu.edu.cn).

Materials availability

Pitx2-P2A-copGFP and Msx1-P2A-tdTomato mice will be available upon request.

Data and code availability

- scRNA-seq data has been submitted to the GEO database (GSE162413).
- All the analysis code has been deposited to Github and the URL is listed in the key resources table.
- Any additional information will be available upon request from the lead contact.

EXPERIMENTAL MODEL AND SUBJECT DETAILS

Mouse strains and animal care

All animal experiments were approved by the Institutional Animal Care and Use Committee at the College of Life Sciences, Sichuan University. All animals were maintained under standardized conditions with the temperature- and light-controlled (12hr light/dark cycle), in individually ventilated cages always with companion mice, and had free access to food and water. Knock-in transgenic mice ($Pitx2^{P2A\text{-}copGFP}$ and $Msx1^{P2A\text{-}tdTomato}$) and $ROSA26^{LSL\text{-}tdTomato}$ mice were custom-generated by Biocytogen, Inc (Beijing). $Sox9^{IRES-CreERT2}$ mice were kindly provided by Prof. Ting Chen from the National Institute of Biological Sciences in China. Sox9-EGFP mice were purchased from the Jackson Laboratory (JAX) (Stock No:030137). After weaning, mice over 8wks old were used for mating, and embryo samples were collected according to the indicated experimental stages in the main text.

METHOD DETAILS

Tooth germ isolation and single-cell preparation

The tooth germs were physically separated from the mandibular using dissection needles under a stereo-fluorescent microscope. Tissues surrounding the tooth germs were eliminated and tooth germs were collected into a clean culture plate. Next, the tooth germs were washed twice with D-PBS and incubated with 0.8mL 0.75mg/mL Dispase (Sigma, Cat# D4693-1G) in 1% FBS D-PBS for 20–45 min (E12.5 20 min; E14.5 30 min; E16.5 35 min; PN1 40 min; PN7 45 min). After that, 3mL culture media supplied with 20μL 5mg/mL DNase (Roche, Cat# 10104159001) was used to neutralize the enzymes and prevent cell aggregates. The epithelium and mesenchyme were then separated and dissociated with 0.25% Trypsin-EDTA (ThermoFisher, Cat# 25200072) for 5 min and 9 min respectively in an incubator at 37°C with 5% CO_2. Finally, single-cell suspensions were collected through a 70μm strainer (Corning, Cat# 352350) and centrifuged at 550g for 5min. Cell number and viability were assessed by an automatic cell counter.

Tooth germ reconstitution *in vitro*

3×10^4 epithelial cells (sorted $Pitx2^+$ (GFP^+) cells) and 6×10^4 mesenchymal cells (sorted $Msx1^+$ ($tdTomato^+$); $Msx1^+Sdc1^+$; $Msx1^+Sdc1^-$; $Msx1^+Enpp1^+$; $Msx1^+Enpp1^-$ cells) or 3×10^4 mesenchymal cells ($Sox9^+$; $Sox9^-$ cells) were mixed gently in 1.5mL microcentrifuge tubes. Next, two rounds of centrifugation at 2900 g for 5min at 4°C were applied. The first round was to collect the cell pellet

and the second was to coat the cell pellet with 20 μL collagen. Then the microtubes were incubated in the incubator at 37°C with 5% CO_2 for another 30min to solidify the collagen. After that, the collagen-coated cell pellet was transferred into the culture plates with ES culture medium (DMEM +15% FBS +1,000U/mL LIF (Novoprotein, Cat# C017). Having cultured overnight, the coated cell pellet was transplanted into the kidney capsule of the recipient mice.

Renal capsule transplantation

The reconstituted tooth germs were isolated from collagen and transplanted into the left renal capsule of the 8-week-old male C57/BL6 mice (Dashuo Experimental Animal Co. Ltd., Chengdu, China). For each mouse, up to 5 samples were transplanted into the host. All the grafts were collected 2–4 weeks after transplantation, fixed with 4% paraformaldehyde, scanned with Micro-CT, and decalcified with 10% EDTA for 2 weeks before further analysis.

Micro-computed tomography (Micro-CT) analysis

The grafts in Figure 2 were radiographed using the μCT50 system (Scanco Medical, Bassersdorf, Switzerland) with a spatial resolution of 5μm (70 kVp, 200μA, 300 ms integration time). 3D imaging reconstruction was calculated after defining the region of interest between the threshold from 220–1000 with the accompanying Micro-CT system software. All the other grafts were trimmed and scanned using the SkyScan 1176 desktop X-ray Micro-CT System (Skyscan, Bruker). Each specimen was placed in a midsized sample holder and a high-resolution scan with an Image Pixel Size of 17.75μm was recorded (60 kV, 410μA, 240ms integration time). Scanning was completed by 360 rotation around the vertical axis, with a rotation step of 0.500, using a 0.5mm Al filter. The scanned images were saved as TIFF files. And these projected images were reconstructed to a BITMAP file using the SkyScan NRecon (SkyScan, Bruker) cone beam reconstruction software. Subsequently, two-dimensional (2-D) images and three-dimensional (3-D) images were obtained using the DateView and CT-Vox software (SkyScan, Bruker), respectively.

Tissue sections and histological analysis

All the samples were dehydrated in 15% and 30% sucrose solution overnight respectively and then pre-treated in the mixture of 30% sucrose solution and OCT (optimal cutting temperature) compound for 1hr before final embedding in the OCT. All the samples were sectioned at 6μm thickness with the microtome cryostat (Leica M1950). Tissue sections were stored at −20°C before being used in histological analysis. For the histological analysis, sections were re-hydrated in PBS for 10 min to remove the OCT compound and then stained with H&E according to the manufacturer's protocol. The bright-filed pictures were captured with the microscope (Olympus, BX43, Japan).

Immunofluorescence for tissue sections

For the immunofluorescence staining, after being re-hydrated in PBS for 10 min to remove the OCT compound, the frozen sections were permeabilized with 0.3% Triton X-100 for 8 min (permeabilization was not performed when analyzing cell surface antigens), and treated by 1× quick antigen retrieval solution (KeyGen Biotech, Cat# KGIHC005) for 5 min at room temperature for antigen retrieval and washed three times with PBS immediately (Gibco, Cat# C10010500BT). Then, the sections were blocked by 5% BSA (Sigma, Cat# A3311-10G) in PBS for 1 h at room temperature and incubated overnight at 4°C with primary antibodies diluted in 2.5% or 5% BSA in PBS according to the manufacturer's suggestion. Secondary antibodies were stained for 1 h at room temperature protected from light and then washed three times with PBS before 4′,6-diamidino-2-phenylindole staining (DAPI) (Thermo Fisher, Cat# D1306) for 5 min. Finally, the sections were enveloped with DAPI-containing mounting medium and examined under a fluorescence confocal microscope (Olympus FV1200, Japan). The RNAscope staining process was carried out according to the manufacturer's instructions. After the staining was completed, the immunofluorescence staining was done as mentioned above. All the antibodies and RNAscope probes were listed in STAR Methods section.

Fluorescence-activated cell sorting (FACS)

Cells were counted with Cell Counter (ThermoFisher) and washed twice with ice-cold D-PBS containing 2% FBS. Cells were incubated with the fluorescent dye-labeled antibody for 20 min on ice, protected from light. Cells were then washed twice with ice-cold DPBS containing 2% FBS and resuspended with D-PBS. Recommended isotype IgG was used as the negative control. All the analysis and sorting were applied by BD Aria III (BD Biosciences, USA).

Culture of the tooth germ organoid

Tooth germs were first reconstituted *in vitro* using (sorted) epithelial and mesenchymal cells. After that, they were cultured in the ES medium (DMEM with 1,000U/mL LIF (Novoprotein, Cat# C017), 15% FBS (Gibco, Cat# 10099–141), 1% NEAA (Gibco, Cat# 11140050), 1% Pen-Strep (Gibco, Cat# 15140122), 1% Glutamax (Gibco, Cat# 35050061), 0.1 mM 2-Mercaptoethanol (Sigma, Cat# M3148)) overnight and then switched to the No-LIF culture medium (DMEM with 15% FBS (Gibco, Cat# 10099–141), 1% NEAA (Gibco, Cat# 11140050), 1% Pen-Strep (Gibco, Cat# 15140122), 1% Glutamax (Gibco, Cat# 35050061), 0.1 mM 2-Mercaptoethanol (Sigma, Cat# M3148). The culture medium was refreshed every other day. The morphology and fluorescence of the tooth germ organoids could be observed directly under the fluorescence microscope (Olympus, IX73, Japan) or confocal microscope (Olympus FV1200, Japan). The formation of enamel requires suspension culture and vitamin C, which means that the tooth

germ needs to be carefully transferred to the Transwell palate (Corning, 3402). 500μL per well No-LIF medium contained 100μg/mL L-ascorbic acid (Sigma, A4403) was added to the plate and the medium was changed every two days. After 24 days, the enamel was identified by H&E staining.

Single-cell preparation and scRNA sequencing

The mandibular tooth germs of E12.5, E14.5, E16.5, PN1(neonatal mice at postnatal day 1), and PN7 were prepared. There were about 20 tooth germs in each period. Primary tooth germs were dissociated into single cells first and resuspended in 1x D-PBS with 1% BSA. Then the sorted mesenchymal and epithelial cells were both counted and adjusted to the concentration of about 1×10^6/ml. Next, the mesenchymal and epithelial cells were mixed at a ratio of 1:2. Then suspension was centrifuged at 550g for 5 min at 4°C and repeated twice. Cells were counted and cell viability was confirmed by Countess II Automated Cell Counter (Thermo Fisher, Cat# AMQAX1000). Samples were then used for single-cell RNA sequencing with the 10x Genomics system (Library preparation and sequencing were performed by Berry Genomics Inc, Beijing). Information and test results of important steps such as single-cell processing, capture, cDNA purification, amplification, library construction, and library purification were recorded in the table.

Parameters	E12.5	E14.5	E16.5	PN1	PN7
Load cell count	12000	12000	12000	12000	12000
Average suspension concentration (cells/μ L)	503	900	999	927	799
Mean cell viability	93.5%	85.0%	88.0%	90.0%	84.8
PCR cycles	12	11	10	12	11
Library concentration (ng/μL)	15.4	25.0	33.2	24.8	22.4
Library size	433	500	502	464	470
Total library(ng)	539	851	1129	868	784
Sample Index	X19	X51	X73	X08	X04

Lineage tracing of Sox9$^+$ cells

ROSA26$^{Loxp-STOP-Loxp-tdTomato}$ mice were mated with Sox9^{CreERT2} male mice and received single or double injections of 1mg/10g bodyweight tamoxifen (Sigma, Cat# T5648) at designated dates. Tooth samples were collected according to the experimental design for evaluation. After fixation overnight at 4°C with 4% PFA, frozen sections were made after dehydration with sucrose. Immunostaining with anti-tdTomato and imaging analysis was then performed. In the *in vitro* culture experiments of the tooth germs, E13.5/14.5 tooth germs were harvested. Whole tooth germs at E13.5 were cultured in a Petri dish. Tooth germs at E14.5 were digested into single cells and used for tooth reconstitution (see organoid culture method for detailed steps). The culture medium with 1.5μM 4-hydroxy tamoxifen (4-OHT, Sigma, 579002) was added for *in vitro* culture. The tooth germ was washed with PBS three times after 24hr to remove 4-OHT and refreshed with the new No-LIF medium without 4-OHT. The culture medium was refreshed every other day. Samples were collected every two days for the frozen sectioning. Frozen sections of tooth germs immunostained with anti-tdTomato were detected by a slide scanner (Olympus VS200, Japan).

Quantitative PCR

Total RNAs were extracted from cells using TRIzol (ThermoFisher, Cat# 15596026) and then reverse-transcribed to cDNA with the Superscript II (ThermoFisher, Cat# 18064014) according to the manufacturer's protocol. The quantitative PCR was performed using a Quant Studio 6 Flex (Applied Biosystems, Foster City, CA, USA) with SYBR Premix Ex Taq (Bio-Rad, USA, Cat# 172–5121), and the relative expression levels were calculated with the comparative threshold cycle (ΔΔCT) method. All tests were performed in triplicate. Primers are listed in Table S1.

Processing of scRNA-seq raw sequencing data

The CellRanger software was obtained from the 10x Genomics website (https://support.10xgenomics.com/single-cell-gene-expression/software/downloads/latest). Alignment, filtering, barcode counting, and UMI counting were performed with cellranger count module to generate a feature-barcode matrix and determine clusters. scRNA-seq data has been submitted to the GEO database (GSE162413).

Reduction, clustering, and identification of differentially expressed genes

The feature-barcode matrix was subsequently processed using R and Seurat v3.0 package. Doublets were scored by Scrublet, and cells were filtered out with scores greater than the "Max doublet score" threshold for downstream analysis. We filtered out cells that have unique features over the "Min number of features" threshold and have counts over the "Min number of counts" threshold and

have mitochondrial counts percentage over the "Max percentage of mitochondrial genes" threshold. Cells that express both *Pitx2* and *Msx1* in one cell are also considered to be low-quality cells. Subsequently, low-quality genes were identified as being expressed in less than 3 cells. The gene expression levels for each cell were normalized by the total expression, multiplied by a default size factor of 10000, and log-transformed. Cell cycle effects were regressed with Seurat's function "ScaleData" using cell cycle markers. The first "No. of principal components" was used to cluster based on a shared nearest neighbor modularity optimization-based clustering algorithm with default parameters. t-SNE (t-Distributed Stochastic Neighbor Embedding) embedding was used to visualize data in reduced dimensions. Differentially expressed genes across cell clusters in each stage were identified with the "FindMarkers" function of Seurat. To identify cell-cluster-specific gene markers, we selected genes that were differentially expressed in clusters with LogFoldchange >0.5 between that cluster and all other clusters at each stage. The top 50 DEGs for different cell clusters were updated in Table S2.

Parameters for processing scRNA-seq data

Parameters	E12.5	E14.5	E16.5	PN1	PN7
Sequencer	HiSeq X	MiSeq	HiSeq X	HiSeq X	HiSeq X
Min number of features	2500	1500	1500	1100	1800
Min number of counts	5000	3500	4000	4000	5000
Max percentage of mitochondrial genes	10%	10%	20%	10%	15%
Max doublet score	0.2	0.2	0.2	0.2	0.2
No. of principal components	14	22	20	26	30

Spatial mapping of gene expression

Spatial mapping of dental genes at E14.5 was done using the DistMap method. Briefly, existing immunohistochemistry (IHC), immuno-fluorescence (IF) and *in situ* hybridization (ISH) data of dental marker genes (in total 103 genes used in E14.5 spatial mapping) were quality-checked before further extracted from published documents for downstream digitalization. The continuous gene expressions of the 103 genes were binarized into two states: expression (ON) and non-expression (OFF), followed by spatial mapping. The tooth model at E14.5 was converted to 50 × 50 grids (2500 bins) as the spatial mapping reference. Digitalized spatial matrixes were drawn according to the specific expression pattern of those digitalized dental markers. The final reference tooth model and binarized expression were included in Figure S8.

Next, the gene correlation matrix of the 103 genes with their binarized versions was computed. For a given gene and the cells expressing it, a quantile was computed, above which the gene would be set to ON, or below to OFF. A given cell was compared to all bins by counting the number of genes found ON or OFF in both the cell and a given bin. In each cell-bin combination, we interpreted the OFF-OFF cases as true negatives (tn), the ON-OFF cases as false positives (fp), the OFF-ON cases as false negatives (fn), and the ON-ON cases as true positives (tp). Mathews correlation coefficient (MCC) was employed to calculate the confusion matrices and assign a cell-bin score: $MCC = \frac{tp \times tn - fp \times fn}{\sqrt{(tp+fp)(tp+fn)(tn+fp)(tn+fn)}}$. The quantiles to maximize MCC scores were used to binarize expressions in single-cell data. For visualization of the vISH results, the reference E14.5 tooth model was used to depict the computed expression patterns. The grey-to-red color scale showed low to high expression per bin.

Molar data integration

Molar scRNA-seq data of E12.5, E14.5, E16.5, PN1, and PN7 were integrated into a whole dataset according to Seurat's manual. Briefly, all epithelial and mesenchymal cells were first extracted for integration. Top 2000 features were selected for finding "anchors" by Seurat's function "SelectIntegrationFeatures". The cells were integrated along the resulting "anchors". The integrated molar data were then scaled, clustered, and dimension reduced as mentioned above. Clustering results were visualized using UMAP.

Pseudotemporal trajectory analysis

Pseudotemporal ordering of molar data was built using R and Monocle 2 algorithms. Using the VariableFeatures function from Seurat and the differentialGeneTest function to select the differential expressed genes, and then standard reduceDimension and orderCells functions were performed to generate the trajectories, and the marker gene expression for each stage was visualized. Subsequently, the VECTOR algorithm (Zhang et al., 2020) was also used for the single-cell data in two stages (E12.5 and E14.5) with a standard protocol with default parameters. The estimation of the trajectory root was based on cluster identities and marker gene analysis. Analysis of the genes switching on and off along the pseudotime was performed using the GeneSwitches package (https://doi.org/10.1093/bioinformatics/btaa099)

CytoTRACE and cellRank analysis

CytoTRACE (https://cytotrace.stanford.edu/) and CellRank (https://cellrank.readthedocs.io/en/stable/) analyses were utilized in our dataset. CytoTRACE analyzed the number of expressed genes per cell and other factors (distribution of mRNA content and number of RNA copies per gene) to predict the differentiation states of each cell (lowest differentiation and highest developmental potential at 1; highest differentiation and lowest developmental potential at 0). CytoTRACE analysis was performed using default parameters. The directed transition matrix was visualized using the KNN graph as well as the CytoTRACE pseudotime through CellRank. The top 50 genes identified by CytoTRACE were listed in Table S3.

pySCENIC analysis

the pySCENIC was used to investigate the potential changes of $Msx1^{+}Sox9^{+}$ dental follicle niche cells during tooth development. pySCENIC analysis was performed using default parameters in Python and then importing the results from Python into R for visualization.

CellChat receptor-ligand analysis

CellChat was used to evaluate the potential for cell-cell interactions in E14.5 datasets. This was implemented using our scRNA-seq Seurat object in R. CellChat analysis was performed using default parameters.

QUANTIFICATION AND STATISTICAL ANALYSIS

Statistical analysis was performed with SPSS 20.0 software (IBM, USA) or R package ggsignif as indicated in the corresponding figure legends. All data show means. Statistical significance was assessed by independent- samples t-test. $p < 0.05$ was deemed statistically significant.